Contents

1 Introduction to the THERA Book **1**

2 THERA: Electron–Proton Scattering at $\sqrt{s} \sim 1$ TeV **3**

2.1 Introduction 5
2.2 Physics with THERA 7
2.2.1 Low-x physics 7
2.2.2 Proton structure and quantum chromodynamics 15
2.2.3 Searches for new particles or phenomena 25
2.2.4 Resolving the partonic structure of the photon 28
2.3 Experimentation at THERA 32
2.3.1 Collision of TESLA electrons with HERA protons 32
2.3.2 A detector for THERA 38
2.4 Further Options 42
2.4.1 Electron–nucleus scattering 42
2.4.2 Real photon–proton scattering 46
2.4.3 Polarised protons 48
2.5 Summary 51

3 Low-x Physics **64**

3.1 Small-x Evolution of Wilson Lines 64
I. Balitsky
3.1.1 Small-x vs Q^2 evolution. 64
3.1.2 High-energy asymptotics as a scattering from the shock-wave field 66
3.1.3 Regularized Wilson-line operators 72
3.1.4 One-loop evolution of Wilson-line operators 75
3.1.5 BFKL pomeron from the evolution of Wilson-line operators . . 79
3.1.6 Non-linear evolution of Wilson lines as functional integral 82
3.1.7 Nuclear structure functions 87
3.1.8 Conclusion 90
3.2 Perturbative Evolution at Small x 94
G. Altarelli, R.D. Ball and S. Forte
3.2.1 Introduction 94
3.2.2 Duality of small x evolution 95
3.2.3 The Double–Leading expansion 97
3.2.4 Resummation 100

3.2.5 Predictions for THERA 102
3.3 High Density QCD at THERA 108
E. Gotsman, E. Levin, M. Lublinsky, U. Maor,
E. Naftali and K. Tuchin
3.3.1 Introduction: Our hopes and main goals at THERA 108
3.3.2 Our model 113
3.3.3 Predictions for THERA 116
3.3.4 Resume 124
3.4 Small x Physics and Forward Jet Production at THERA 130
H. Jung and L. Lönnblad
3.4.1 Introduction 130
3.4.2 Initial State QCD Cascade 132
3.4.3 Conclusion 134
3.5 Gluon Saturation and the Color Glass Condensate 137
E. Iancu and L. McLerran
3.5.1 Introduction 137
3.5.2 The Color Glass Condensate 138
3.5.3 Quantum evolution and BFKL 141
3.5.4 The quantum evolution of the CGC 143
3.5.5 Recovering some known results 147
3.5.6 Solving the RGE: Saturation and Universality 148
3.6 Saturation at low $\mathbf{x}$ 161
E. Levin
3.6.1 Introduction 161
3.6.2 Qualitative Picture of Interaction in DIS at low $\mathbf{x}$ 162
3.6.3 Non-linear Evolution 170
3.6.4 Initial conditions: 173
3.6.5 Saturation scale $\mathbf{Q_s(x)}$ 174
3.6.6 A new scaling in the saturation region. 176
3.6.7 Parton densities at THERA and LHC energies 179
3.6.8 Summary 181
3.7 Saturation and Unitarity of Hadronic Structure Functions 187
Yu.V. Kovchegov
3.7.1 "Phase Diagram" of High Energy QCD 187
3.7.2 Qualitative Picture of Saturation 188
3.7.3 Evolution equation from the dipole model 191
3.7.4 Double Logarithmic Limit 197
3.7.5 Approximate Solution of the Nonlinear Evolution Equation . . . 199
3.7.6 Asymptotic Behavior of the F_2 Structure Function 204
3.7.7 Diffractive Dissociation Including Multiple Pomeron Exchanges 206
3.8 Diffractive Production of Neutral Vector Mesons 213
J.A. Crittenden
3.8.1 Introduction 213
3.8.2 Lessons from HERA 216

3.8.3 Requirements on the performance of machine and detector . . . 219
3.8.4 Conclusions 221

4 Proton Structure and Quantum Chromodynamics 226
4.1 Heavy Quark Production Measurements at THERA 226
L. Gladilin and I. Redondo
4.1.1 Introduction 227
4.1.2 Heavy quark photoproduction and proton gluon structure 228
4.1.3 Heavy quark production in neutral current DIS 231
4.1.4 Charm production in charged current DIS 237
4.1.5 Summary 239
4.2 High-p_T Jet Production 242
B. Pötter
4.2.1 Introduction 242
4.2.2 Next-to-leading order calculations 242
4.2.3 Jet Production at THERA 243
4.2.4 Summary 246
4.3 Jet Photoproduction at THERA 249
M. Klasen
4.3.1 Motivation 249
4.3.2 Dijet Cross Section 250
4.3.3 Results 251
4.3.4 Conclusion 255
4.4 Precision Tests of Perturbative QCD at THERA 258
W.L. van Neerven
4.4.1 Introduction. 258
4.4.2 Light cone dominance and sum rules. 259
4.4.3 Heavy flavour production. 264
4.4.4 Comparison between electro-production and photo- and hadro-production. 269
4.5 Heavy Quark Production in the Semihard QCD Approach at THERA . 274
S.P. Baranov and N.P. Zotov
4.5.1 Introduction 274
4.5.2 The semihard QCD approach 275
4.5.3 Numerical results 278
4.6 Charged-current Deep Inelastic Scattering at THERA 285
K. Nagano
4.6.1 Introduction 285
4.6.2 Double differential cross-section measurement 286
4.6.3 The d-quark density at high-x 287
4.6.4 Determination of the propagator mass 288
4.6.5 Summary 289

5 Searches for New Particles or Phenomena 290
5.1 Contact Interactions, Large Extra Dimensions and Leptoquarks 290
A.F. Żarnecki
5.1.1 Contact Interactions 290
5.1.2 Large Extra Dimensions 291
5.1.3 Leptoquarks 292
5.1.4 Analysis method 296
5.1.5 THERA running 298
5.1.6 Results 298
5.1.7 Summary 303
5.2 Pair Production of Supersymmetric Particles 313
M. Corradi
5.2.1 Introduction 313
5.2.2 Selectron and Squark Production 314
5.2.3 Selectron and Neutralino Production 316
5.2.4 Conclusions 316
5.3 Search for Excited Fermions at THERA 318
M. Kuze
5.3.1 Introduction 318
5.3.2 Results 318
5.3.3 Conclusions 319

6 Resolving the Partonic Structure of the Photon 321
6.1 Reach of Future Colliders in Probing the Structure of the Photon . . . 321
M. Krawczyk, S. Söldner-Rembold and M. Wing
6.1.1 Introduction 321
6.1.2 The THERA kinematic region in comparison with other colliders 323
6.1.3 Summary 324
6.2 Inclusive Dijet Photoproduction and the Resolved Photon at THERA . 326
M. Wing
6.2.1 Introduction 326
6.2.2 Photoproduction from HERA to THERA 328
6.2.3 Cross section definition 329
6.2.4 Results 330
6.2.5 Discussion 332
6.2.6 Summary 335
6.3 Heavy Quark Photoproduction at THERA 338
P. Jankowski, M. Krawczyk and M. Wing
6.3.1 Introduction 338
6.3.2 Leading order QCD predictions of charm quark production . . . 339
6.3.3 MC predictions of dijet production with charm and beauty quarks342
6.3.4 Summary 345
6.4 The Prompt Photon Photoproduction at THERA 349
M. Krawczyk and A. Zembrzuski

6.4.1 Introduction 349
6.4.2 The NLO cross section 349
6.4.3 The results 352
6.4.4 Summary 353
6.5 On the Importance of the Contribution of the Longitudinal Virtual Photon... 355
U. Jezuita-Dąbrowska and M. Krawczyk
6.5.1 Introduction 355
6.5.2 Factorisation of the one-photon exchange cross sections for the inclusive and semi-inclusive unpolarised lepton-nucleon scattering 357
6.5.3 Azimuthal angle distribution for the semi-inclusive process . . . 360
6.5.4 Numerical results 361
6.5.5 Conclusions 365

7 Electron-Nucleus Scattering 371
7.1 Electron-Nucleus Collisions at THERA 371
L. Frankfurt, V. Guzey, M. McDermott and M. Strikman
7.1.1 Executive Summary 371
7.1.2 Introduction 372
7.1.3 The black body limit and its signals in DIS final states 377
7.1.4 Unitarity constraints for electron-nucleus DIS 386
7.1.5 Nuclear shadowing and diffraction 389
7.1.6 Experimental considerations 400
7.1.7 Conclusions 401

8 Real Photon-Proton Scattering 405
8.1 Gamma Options of the THERA Collider 405
O. Çakir, A. K. Çiftçi, S. Sultansoy, Ö. Yavaş and M. Yilmaz
8.1.1 Introduction 405
8.1.2 Luminosity considerations 405
8.1.3 Physics goals 407

2 THERA: Electron–Proton Scattering at $\sqrt{s} \sim 1$ TeV

A Contribution to the TESLA Technical Design Report
13. Feb. 2001

H. Abramowicz[41], S.P. Baranov[21], J. Bartels[17], W. Bialowons[13], R. Brinkmann[13], O. Çakır[4], A. Caldwell[12], V. Chekelian[32,31], A.K. Çiftçi[4], J.G. Conteras[14], M. Corradi[7], J.A. Crittenden[8], J. Dainton[23], K. Daum[45], A. Deshpande[46,39], D. Eckstein[13], E. Elsen[13], B. Foster[9], L. Frankfurt[41], E. Gabathuler[23], J. Gassner[38], U. Gensch[13], I. Ginzburg[33], L. Gladilin[44], M. Glück[14], N. Gogitidze[21], K. Golec-Biernat[17], E. Gotsman[41], T. Greenshaw[23], V. Guzey[2], P. Jankowski, U. Jezuita-Dabrowska[42], H. Jung[13], U.F. Katz[8], R. Klanner[13,17], M. Klasen[17], M. Klein[13], B. Kniehl[17], H. Koru[5], P. Kostka[13], H. Kowalski[13], M. Krawczyk[42], T. Kurča[20], M. Kuze[19], P. Landshoff[10], T. Laštovička[37], B. Levchenko[30], E. Levin[41], A. Levy[41], K. Long[24], L. Lönnblad[25], U. Maor[41], M. McDermott[23], K. Nagano[19], T. Naumann[13], W. van Neerven[22], P. Newman[6], N. Nikolaev[18], C. Pascaud[34], E. Perez[40], D. Pitzl[13], B. Pötter[32], G. Rädel[1], V. Ravindran[3], I. Redondo[26], E. Reya[14], A. De Roeck[11], E. Rondio[43], J. Ruan[15], W. Schäfer[18], S. Schlenstedt[13], P. Schleper[13], U. Schneekloth[13], S. Söldner-Rembold[16,11], H. Spiesberger[27], U. Stösslein[13], M. Strikman[36], S. Sultansoy[5], K. Tuchin[41], W.K. Tung[29], R. Wallny[47], D. Waters[35], P. Wesolowski[13], F. Willeke[13], M. Wing[28], Ö. Yavaş[4], M. Yılmaz[5], A.F. Żarnecki[42], A. Zembrzuski[42], A. Zhokin[31], V. Zoller[31], N.P. Zotov[30]

[1] RWTH Aachen, Germany
[2] University of Adelaide, Australia
[3] Mehta Research Institute of Mathematics and Mathematical Physics, Allahabad, India
[4] Ankara University, Turkey
[5] Gazi University, Ankara, Turkey
[6] University of Birmingham, UK
[7] INFN Bologna, Italy
[8] Universität Bonn, Germany
[9] University of Bristol
[10] Cambridge University, UK
[11] CERN, Geneva, Switzerland
[12] Columbia University, Nevis Labs, Irvington, USA
[13] DESY, Hamburg and Zeuthen, Germany
[14] Universität Dortmund, Germany
[15] East China Normal University, Shanghai, P.R. China
[16] Universität Freiburg, Germany
[17] Universität Hamburg, Germany
[18] Forschungszentrum Jülich, Germany
[19] KEK, Tsukuba, Japan
[20] Institute of Experimental Physics, Košice, Slovak Republic
[21] Lebedev Physical Institute, Moscow, Russia
[22] University of Leiden, The Netherlands
[23] University of Liverpool, UK
[24] Imperial College London, UK
[25] Lund University, Sweden
[26] Universidad Autónoma de Madrid, Spain
[27] Universität Mainz, Germany
[28] McGill University, Montreal, Canada
[29] Michigan State University, East Lansing, USA
[30] Moscow State University, Russia
[31] ITEP, Moscow, Russia
[32] MPI für Physik, München, Germany
[33] Institute of Mathematics, Novosibirsk, Russia
[34] LAL, Orsay, France
[35] University of Oxford, UK
[36] Pennsylvania State University, New Kensington, USA
[37] Charles University, Prague, Czech Republic
[38] PSI, Villingen, Switzerland
[39] RIKEN-BNL Research Center, Upton, USA
[40] DAPNIA-CEA/Saclay, Gif sur Yvette, France
[41] Tel Aviv University, Israel
[42] Warsaw University, Poland
[43] Institute for Nuclear Studies, Warsaw, Poland
[44] Weizmann Institute, Rehovot, Israel
[45] Universität Wuppertal, Germany
[46] Yale University, New Haven, USA
[47] Universität Zürich, Switzerland

2.1 Introduction

The elementary nature of the electron makes it a good probe to study the structure of the proton in deep inelastic *ep* interactions [1]. Previous fixed-target deep inelastic scattering (DIS) experiments have discovered the partonic structure of the nucleon and established Quantum Chromodynamics (QCD) as the correct field theory of quark–gluon interactions at small distances.

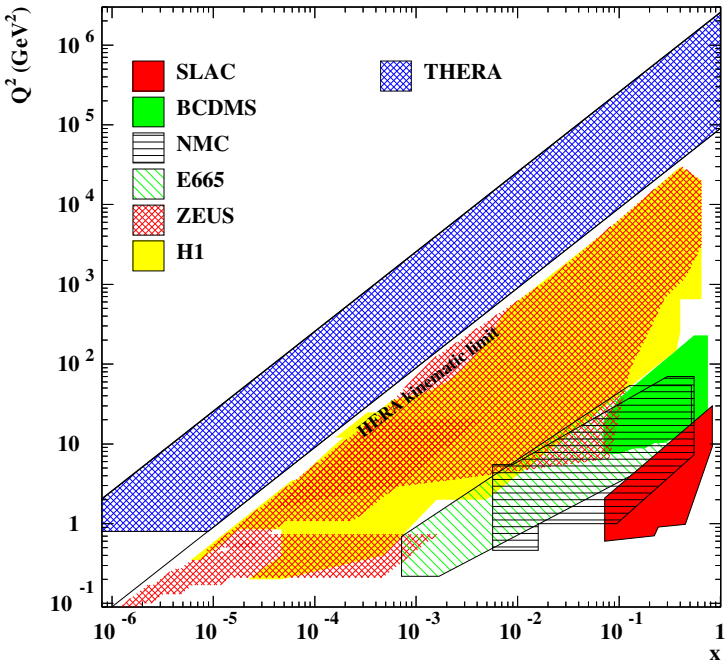

Figure 2.1.1: *The kinematic plane in deep inelastic lepton–proton scattering, showing the regions covered by fixed-target scattering experiments and by the HERA experiments, and the extension of the kinematic range by the THERA collider with an ep centre-of-mass energy squared of* $s = 2.56 \times 10^6\ GeV^2$. *The variables* x *and* Q^2 *denote the Bjorken scaling variable and the negative square of the four-momentum transfer between lepton and proton, respectively.*

HERA [2], the first electron–proton collider, has been a major step forward in accelerator technology and has resulted in a number of fundamental physics observations: the discovery of the rise of the proton structure function $F_2(x, Q^2)$ towards low Bjorken x, which is related to a large gluon density in the proton; the discovery of hard diffractive scattering in DIS and the confirmation of the pointlike nature of the partons down to distances of about 10^{-18} m. The HERA measurements at low Q^2 have initiated intense studies of the transition between QCD radiation at small distances and non-perturbative parton dynamics at large transverse distances, which has become a central issue in modern strong interaction theory.

THERA[1] uses polarised electrons or positrons from the linear accelerator TESLA at energies of 250–800 GeV and brings them into collision with high-energy protons (500 GeV to 1 TeV) from HERA in the West Hall on the DESY site. THERA will thus extend the investigation of deep inelastic scattering into an as yet unexplored kinematic region (Fig. 2.1.1), yielding complementary information to hadron–hadron and e^+e^- colliders in the TeV energy range.

At low x, THERA offers the possibility of uncovering a new strong-interaction do-

[1] The acronym THERA symbolises a combination of TESLA and HERA. It also is the name of a Greek island, which in the Doric period was called Kalliste, most beautiful.

main of parton saturation, which would be a substantial step towards an understanding of confinement. Processes such as jet production in the proton beam direction or heavy flavour production at low x, studies of the partonic structure of the photon and a precision measurement of the strong interaction coupling constant α_s make THERA an excellent facility for investigating strong and electroweak interaction dynamics. Finally, the high centre-of-mass energy will open a new window for the observation of new particles or interactions, such as leptoquarks, supersymmetric particles or contact interactions, the helicity structure of which could be particularly well investigated at THERA.

With centre-of-mass energies beyond 1 TeV, structures in the proton with sizes down to 10^{-19} m will be resolved. In the history of the exploration of the basic structure of matter, illustrated in Fig. 2.1.2, THERA thus represents a new major step.

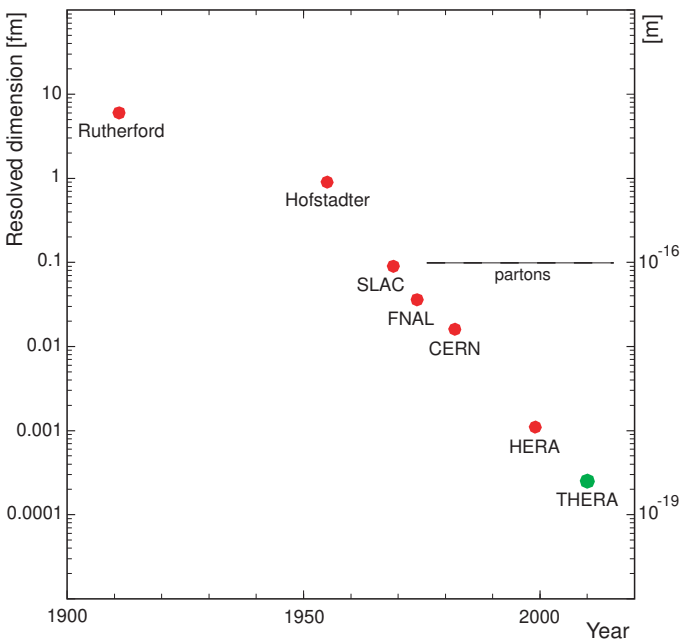

Figure 2.1.2: *The development over time of the resolution power of experiments exploring the inner structure of matter, from the Rutherford experiment to THERA.*

The electron–proton scattering programme at THERA can be greatly extended by accelerating nuclei or polarised protons in the HERA ring, or with real photon–proton scattering using laser light backscattered off the electron beam. Thus THERA can be a unique long-term, cost-effective facility for inelastic lepton–hadron scattering in an unexplored range.

The structure of this appendix[2] is the following: In Sect. 2.2 the physics subjects studied are discussed, and the major physics possibilities are highlighted. In Sect. 2.3 the THERA machine layout and luminosity estimates, as well as the concept of a THERA detector, are presented. Sect. 2.4 presents briefly the physics options of running the THERA facility in $\vec{e}A$, $\vec{\gamma}p$ and $\vec{e}\vec{p}$ mode. A brief summary is given in Sect. 2.5.

[2]This appendix summarises studies of a group of about one hundred physicists. Most of the results are available on the web (`http://www.ifh.de/thera`) and will be documented in more detail in a separate volume [3].

2.2 Physics with THERA

2.2.1 Low-x physics

From the measurement of the differential cross section $d^2\sigma/dx\,dQ^2$ in inclusive deep-inelastic lepton–proton scattering, $\ell p \to \ell X$, the proton structure function $F_2(x, Q^2)$ is determined. In the naive Quark Parton Model (QPM), F_2 is interpreted as the sum of the momentum densities of quarks and anti-quarks in the proton, weighted with their charge squares. The variable x is interpreted as the fraction of the proton's longitudinal momentum carried by the struck quark. According to the relation $x = Q^2/sy$ (where y is the fractional energy carried by the exchanged current), every step towards higher centre-of-mass energy, $\sqrt{s}$, leads deeper into the unexplored region of low x.

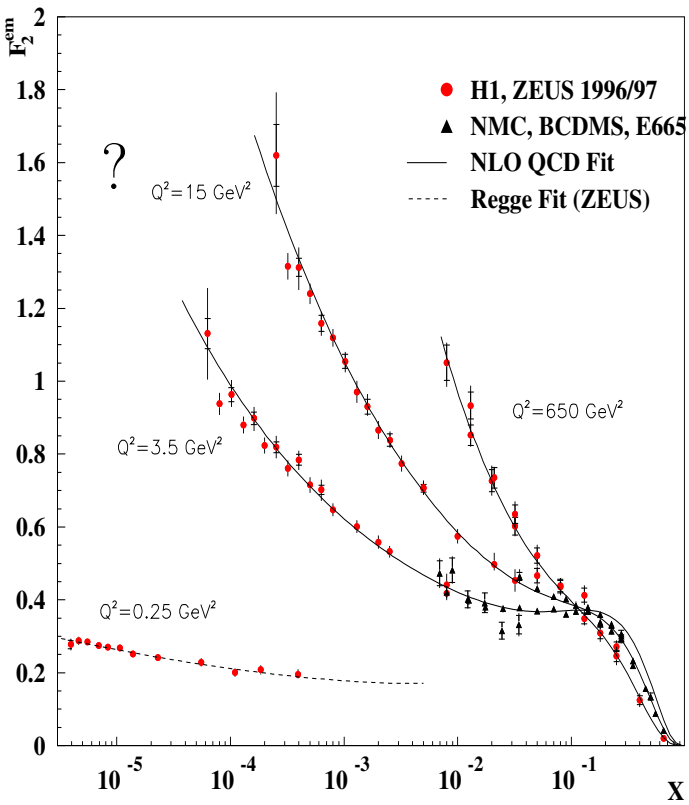

Figure 2.2.1: *The proton structure function $F_2(x, Q^2)$ as measured in fixed-target μp scattering at large x, and in ep scattering at HERA. The solid curves show a fit using the next-to-leading order QCD evolution equations. The dashed curve for the lowest-Q^2 data is a fit using Regge theory. The structure function in the low-x region represents the sea-quark component of the proton. With THERA, the kinematic range will be extended by a further order of magnitude towards lower x. The expected behaviour of F_2 in this new region is hotly debated.*

The high-energy collider HERA and its experiments have extended the kinematic (x, Q^2) region for DIS by about two orders of magnitude. As can be seen in Fig. 2.2.1, the structure function F_2 as measured at HERA [4, 5] and thus the sea-quark density rises by a large factor towards low x, and the increase becomes stronger with increasing Q^2. The data in the DIS region were found to be well described by the QCD evolution equations [6], which are based on the renormalisation group equations and the operator product expansion. Figure 2.2.1 also illustrates that the behaviour of the data [7] at low $Q^2 < 1\,\mathrm{GeV}^2$ is completely different, showing a slower, logarithmic rise, which is typical for the energy dependence of soft hadronic processes.

Much of the understanding of strong interaction dynamics is derived from the study

of Q^2 dependences in DIS. The HERA experiments have found that $F_2(x, Q^2)$ at fixed small values of x strongly rises with Q^2. In the standard QCD evolution equations, the derivative $(\partial F_2/\partial \ln Q^2)_x$ at fixed low x is, at leading order, proportional to the product of the strong interaction coupling constant, α_s, and the gluon momentum density, xg. Thus the rise of F_2 with Q^2 as measured at HERA implies a large gluon density in the proton, which increases towards low x (see Fig. 2.2.2). However, it remains an open question whether the underlying evolution equations strictly hold at the lowest x values, in spite of neglecting large logarithms of the type $\ln(1/x)$ and possible unitarity effects. Data at lower x and larger Q^2 are required to resolve this issue. Theoretical QCD developments regarding DIS at low x are discussed in Sect. 2.2.2.1.

In the HERA collider experiments a number of observables have been studied which provide insight into strong interaction dynamics independently of F_2 and are also sensitive to the behaviour of the gluon distribution at low x. Examples are the longitudinal structure function $F_L \propto \alpha_s xg$ [4], the production of vector mesons like J/ψ [8, 9] ($\propto (\alpha_s xg)^2$) and the charm structure function F_2^c [10, 11]. The successful description of these and further measurements with a single set of parton distribution functions of the proton has been a major success of perturbative QCD.

Due to the high density of quarks and gluons, qualitatively new signatures are expected in the low-x region of THERA. An extrapolation of the rise of F_2 to lower x, as indicated by Fig. 2.2.1, would at some point violate the unitarity limit of virtual photon–proton scattering. An upper limit on xg is obtained from the unitarity re-

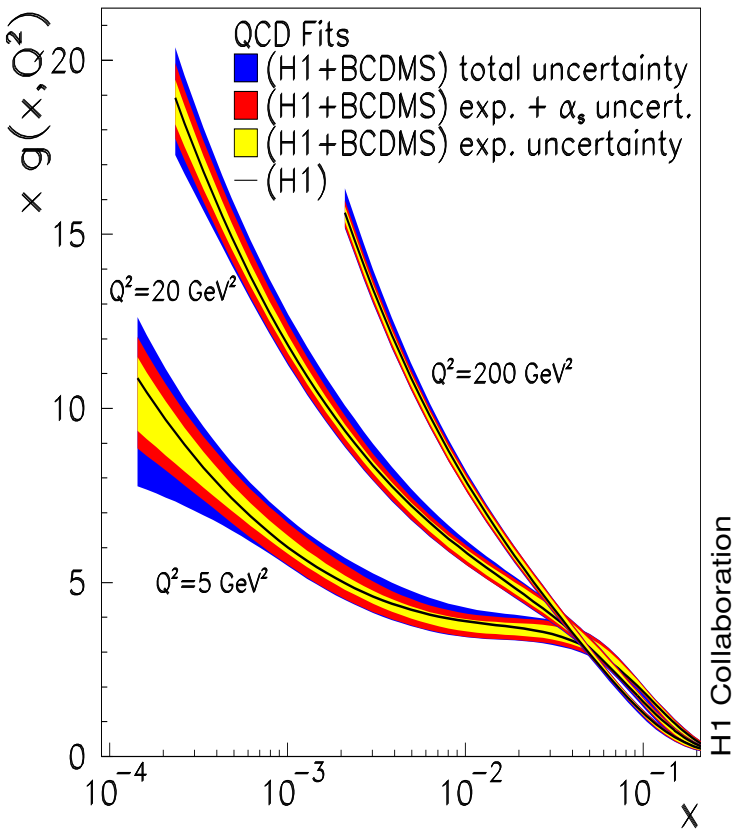

Figure 2.2.2: *Gluon momentum distribution measured at HERA, extracted within the framework of the conventional evolution equations of perturbative QCD. The gluon distribution is sensitive to the understanding of heavy flavour production at low x and Q^2. The behaviour of the gluon density in the kinematic range of THERA is a hotly debated issue which has to be resolved experimentally.*

quirement that the inelastic cross section of the interaction of a small dipole[3] [13–15] with the proton may not exceed the transverse proton size πR^2. This leads to an approximate constraint [16, 17]

$$xg(x, Q^2) \leq \frac{1}{\pi N_c \alpha_s(Q^2)} Q^2 R^2 \simeq \frac{Q^2}{\alpha_s} , \tag{2.2.1}$$

where N_c is the number of colours and Q^2 is given in GeV^2. Given the strong rise of xg towards low x (Fig. 2.2.2), it seems likely that the unitarity limit is reached in the THERA kinematic range and that therefore this rise eventually becomes tamed. As discussed in Sect. 2.4.1, it is possible that these effects are amplified in electron–nucleus scattering. In any case, understanding deep inelastic structure functions in the THERA range is of crucial relevance for the description of high-energy cross sections at hadron colliders and astro-particle physics experiments [18, 19].

Saturation may be connected with a novel, high parton density state of QCD, between the low-density region of partons and the region of confinement. The transition from the perturbative range of small distances to the physics at large distances is currently being intensively studied, using data from the HERA collider experiments on the total virtual-photon proton cross section as well as on elastic vector meson production and diffraction. Despite the success of phenomenological models, however, a consistent theoretical description remains elusive [20][4], and a significant extension of the kinematic range in deep inelastic scattering is required.

2.2.1.1 The high-density QCD phase and confinement

The deep inelastic scattering process can be viewed as a fluctuation of the incoming proton into a cloud of constituents which is subsequently scanned by the virtual photon. The life-time of the cloud, $\tau \approx 1/Mx$, is considerably longer than the photon interaction time (M being the proton mass). Therefore the photon takes 'snapshots' of the 'frozen' proton cloud with a resolution $\Delta r \approx 1/\sqrt{Q^2}$. The x and Q^2 dependence of the proton structure may be viewed as sketched in Fig. 2.2.3.

HERA data and theoretical studies suggest that hadrons have a qualitatively different structure in three domains:

[3] Theoretical descriptions of DIS at low x frequently use a frame in which the proton is at rest. In the high-energy limit, low-x processes factorise into a virtual photon fluctuation to a hadronic system at large distances from the proton target, which is followed by a brief interaction with the target and subsequent hadronic final state formation over a longer period. The simplest fluctuation, which dominates for systems with small transverse size, is a quark–antiquark state which forms a colour-triplet dipole. This view is attractive for describing inclusive DIS at low x as well as suitable for vector meson production and diffractive processes. It has been successfully used and developed much further in recent years, as is reviewed in [12].

[4] This is reminiscent of a situation about 100 years ago before Planck successfully solved the black-body radiation problem bridging the gap between Wien's law and the Rayleigh–Jeans formula. In analogy to the ultraviolet catastrophe, i.e. the divergence of the Rayleigh–Jeans law at small wavelengths, the proton structure function F_2 cannot grow indefinitely as x approaches zero.

1. The *domain of perturbative QCD* with small-size constituents which are distributed in a hadron with rather low density (the region below the solid line in Fig. 2.2.3). Reacting partons are resolved with a resolution determined as $\Delta r \approx 1/Q$.

2. The *QCD domain of high parton density* [21, 22] but small coupling, where the density is too large to use the established perturbative QCD methods (the region above the solid line). Theoretical studies suggest that the size of the partons in this region is effectively determined by an x dependent resolution scale, $Q_S(x)$: $\Delta r \approx 1/Q_S(x)$ [23].

3. The *non-perturbative QCD domain*, in which the QCD coupling α_s is large, Regge theory applies and the confinement of quarks and gluons occurs. New theoretical methods must be developed to explore this region (left of the dash-dotted line).

According to [17, 24] the HERA data suggest the existence of the high-density QCD domain in which a new scaling law for the virtual photon–proton cross section may apply [25]. However, the HERA data can also be described without such an assumption [17, 26]. At THERA, such investigations can be performed at larger Q^2 for a given x, i.e. more safely inside the region of small α_s. Thus the extension of the kinematic range is crucial to the distinction and analysis of these states of matter.

It is well known that in the short-distance limit (i.e. in the perturbative QCD domain), quarks and gluons are the proper degrees of freedom of the QCD Lagrangian. To describe the transition from short to long distances, however, one needs to consider degrees of freedom beyond quarks and gluons. Approaches based on colour dipole formation as the first stage in this transition are promising.

Understanding the confinement of quarks and gluons is still a challenge to theorists. Deep inelastic scattering provides two approaches to study this phenomenon. Firstly,

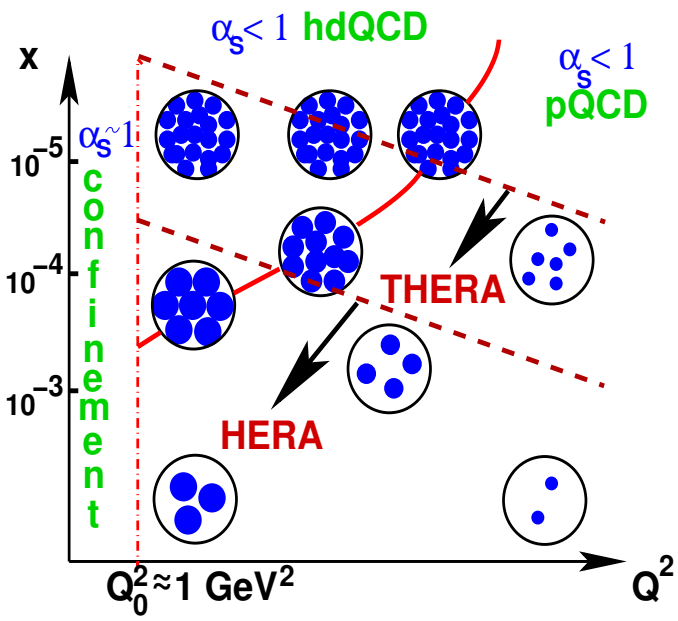

Figure 2.2.3: *Snapshots of the proton constituents (full dots) taken with different resolution ($\Delta r \approx 1/Q$) at different values of x. The solid line shows the estimated position of the transition from the perturbative region to the high-density phase of QCD (hdQCD). The resolution scale diminishes with Q^2 in the pQCD region but with x in the hdQCD region. The vertical dash-dotted line delimits the confinement region. The dashed lines and the corresponding arrows indicate the HERA and THERA measurement ranges. The observation of signatures allowing the identification of the various regions is a challenge for THERA.*

the experimental data at high energies suggest some properties of confinement, such as factorisation, the space-time picture or the quark model. These hint at the effective degrees of freedom and at which type of effective Lagrangian may be used for developing a microscopic theory at high energies. Secondly, DIS data allow the matching of perturbative and non-perturbative QCD domains to be studied by investigating low-Q^2 virtual-photon proton scattering. Clearly, a solution to the confinement problem of hadrons has fundamental implications.

2.2.1.2 Vector-meson production

Investigations of vector meson production at HERA have provided insights into the dynamics of both soft and hard diffractive processes [27] (for a review see [28]). The high flux of quasi-real photons from the electron beam permitted detailed measurements of both elastic and proton-dissociative photoproduction of ρ^0, ω, ϕ, J/ψ, and Υ mesons. Power-law scaling with the photon–proton centre-of-mass energy, W, was observed, as is illustrated by Fig. 2.2.4. The steep energy dependence measured for J/ψ mesons inspired a number of theoretical approaches based on perturbative QCD [29–31].

In the theory of light vector mesons, the photon virtuality [16, 33–36] and the momentum transferred to the proton [37–40] were introduced as hard scales. These calculations demonstrated remarkable sensitivity to the gluon density, since the cross sections were shown to be proportional to $(xg)^2$. With large THERA data samples,

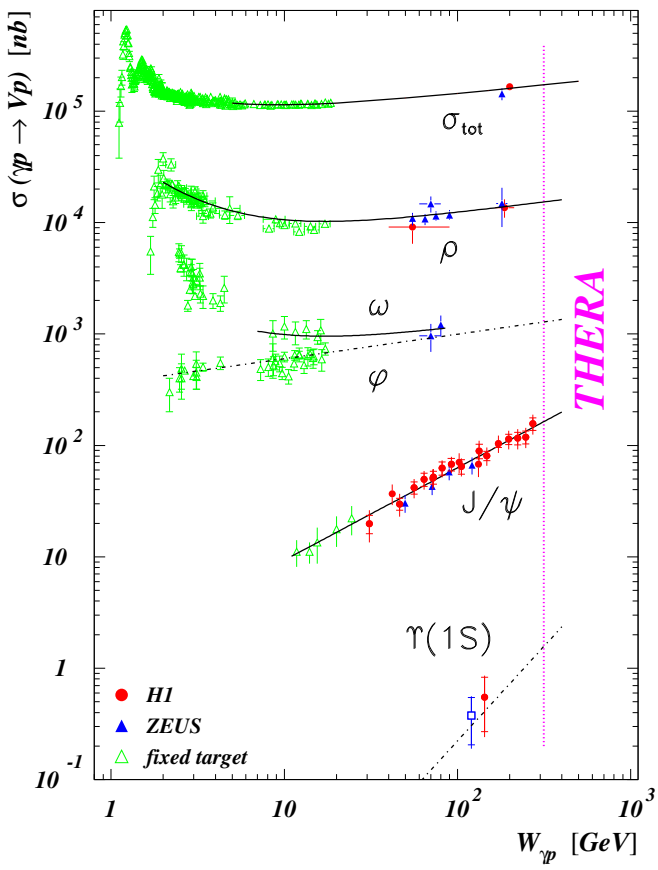

Figure 2.2.4: *Energy dependence of the total γp cross section and the elastic vector meson photoproduction cross sections for ρ^0, ω, ϕ, J/ψ, and Υ mesons. Here W is the photon–proton centre-of-mass energy. The plot is reproduced from [32]. Since the production cross section of heavy vector mesons is proportional to $(xg)^2$, measurements in the THERA range of W up to 1 TeV may be sensitive to saturation.*

covering a variety of vector meson species, remaining theoretical uncertainties can be tackled, such that elastic vector meson production could become a competitive means of extracting the gluon density. Of particular interest is the question whether the rise of the J/ψ cross section towards large W (Fig. 2.2.4) is tamed, for example by unitarity effects, or indeed persists [26]. Because of the enlarged cross section and W range, the investigation of Υ meson production [41, 42] will become an important topic at THERA.

Whereas perturbative QCD is applicable where hard scales are present, long-range strong-interaction dynamics apply to the forward production of light vector mesons at low Q^2. The transition between these two regimes is studied by scanning Q^2 or the square of the four-momentum transfer at the proton vertex, t, allowing comparisons to hadronic interactions. Of particular interest is the possibility of determining the transverse interaction size which may grow with energy [17, 26, 43], as given by the slope of the Pomeron trajectory, α'. Due to the weakness of the energy dependence in such long-distance processes, the extension of the energy reach is essential to provide sensitivity to α'.

The programme of vector meson measurements will benefit not only from the extended kinematic reach but as well from the improved coverage of the THERA detector at small angles and from tagging systems in both the proton and electron beam directions, designed with the benefit of the experience obtained at HERA.

2.2.1.3 Hard diffractive scattering

A striking result at HERA has been the abundance of diffractive processes of the type $ep \to eXp$ [44, 45] in DIS, where the proton remains intact with only a small loss in momentum. Deep inelastic scattering at low x thus became, rather unexpectedly, an important process for the understanding of one of the oldest puzzles of high energy physics, the nature of diffraction [46]. The mechanism responsible for diffraction remains unsettled, and its investigation will profit enormously from the extended phase space available at THERA. Since total, elastic and diffractive cross sections are closely related via the optical theorem, it is clear that a correct description of diffractive processes must be an integral part of any consistent theory of low-x physics [47–49].

The diffractive contribution to F_2 has been measured in the form of a structure function $F_2^{D(3)}(x_{I\!P}, \beta, Q^2)$. Here, as illustrated in Fig. 2.2.5a, $x_{I\!P}$ is the fractional proton longitudinal momentum loss and $\beta = x/x_{I\!P}$ is the fraction of the exchanged longitudinal momentum carried by the quark coupling to the virtual photon. Figures 2.2.5b,c show the kinematic regions in which diffractive processes can be measured at HERA and at THERA. An extension of approximately an order of magnitude towards lower β or $x_{I\!P}$ is obtained at fixed Q^2.

The hard scale supplied by the photon virtuality has encouraged perturbative QCD approaches to diffractive DIS. A QCD factorisation theorem has recently been proven for the process [50], implying that diffractive parton densities at fixed $x_{I\!P}$ can be defined, which should describe both the scaling violations of $F_2^{D(3)}$ and exclusive final state cross sections such as those for high-p_t jet production. HERA data have shown that

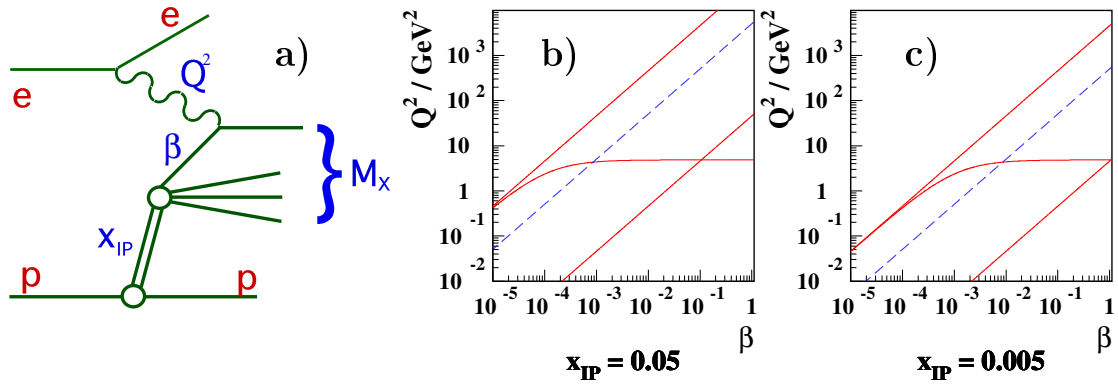

Figure 2.2.5: *(a) Feynman diagram of diffractive ep scattering, with the kinematic quantities indicated in blue. (b,c) The accessible kinematic plane in β and Q^2 for diffractive DIS at two different values of $x_{I\!P}$. The solid red lines show the limits imposed by the cuts $0.001 < y < 1$ and $\theta_e < 179.5°$ for THERA, with electrons of 250 GeV and protons of 920 GeV. The dashed blue lines show the kinematic limit at HERA.*

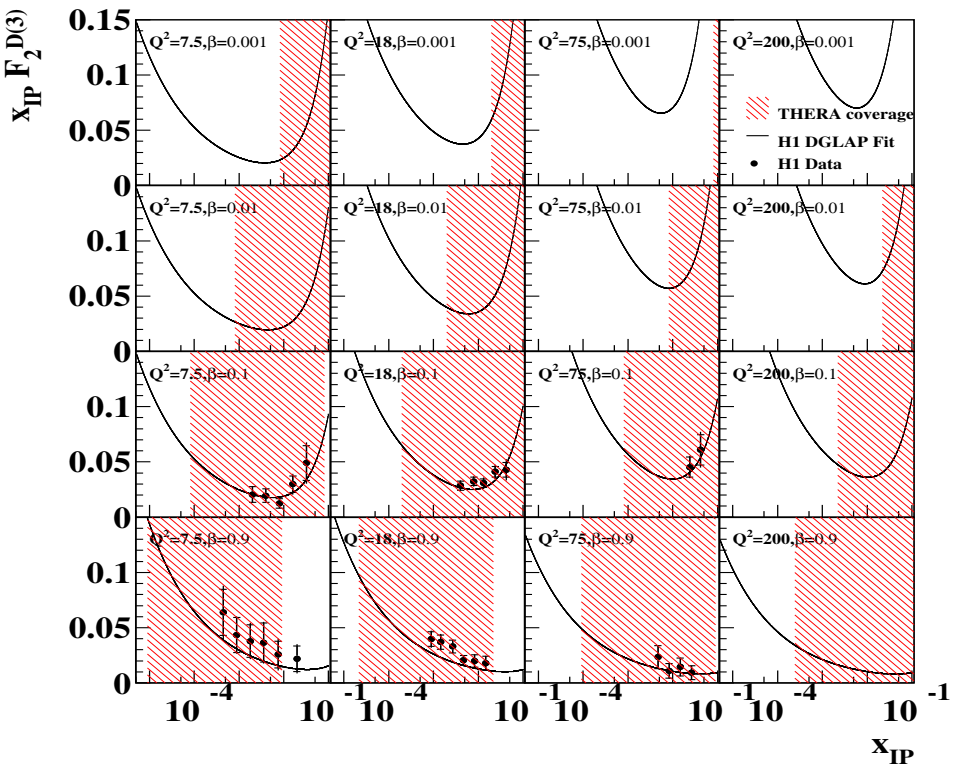

Figure 2.2.6: *Illustration of the kinematic coverage for measurements of $F_2^{D(3)}(x_{I\!P}, \beta, Q^2)$ at HERA and at THERA. The accessible $x_{I\!P}$ range is shown for selected values of β and Q^2. Appropriate HERA data points from [44] are also shown. The curves are extrapolations of QCD fits to data with $\beta < 0.65$ from [44]. The shaded areas show the region of extended coverage at THERA (920 GeV protons, 250 GeV electrons).*

the diffractive parton densities are dominated by gluons at large β [51]. The region $\beta \lesssim 0.05$ remains poorly explored at HERA.

In the proton rest-frame approach, diffractive DIS is considered as the elastic scattering of the proton with $q\bar{q}$ and $q\bar{q}g$ partonic fluctuations of the virtual photon. The scattering has been modelled either in terms of multiple interactions in the non-perturbative colour field of the proton [52, 53] or in terms of the exchange of a pair of perturbative gluons [24, 54, 55]. THERA data in an extended phase space will be very powerful in distinguishing between these different approaches.

From combined analyses of diffractive and inclusive $\gamma^* p$ cross sections, it has been suggested that the regime of parton saturation, expected as the unitarity limit is approached, is already reached at HERA [24]. Diffractive data are crucial for this sort of analysis, since for fixed x, saturation is expected to set in at larger Q^2 values in the diffractive than in the inclusive cross section. Although the presence or absence of saturation effects in diffraction at HERA is hotly debated, it is likely that the effect will be clearly visible in the extended low-x range at THERA.

Figure 2.2.6 indicates the regions in which measurements of $F_2^{D(3)}$ will be possible at THERA, together with selected data points from HERA. Extrapolations of a QCD fit to HERA data [44] based on DGLAP evolution of the diffractive parton distributions are also shown. THERA measurements at lower β will allow the precise determination

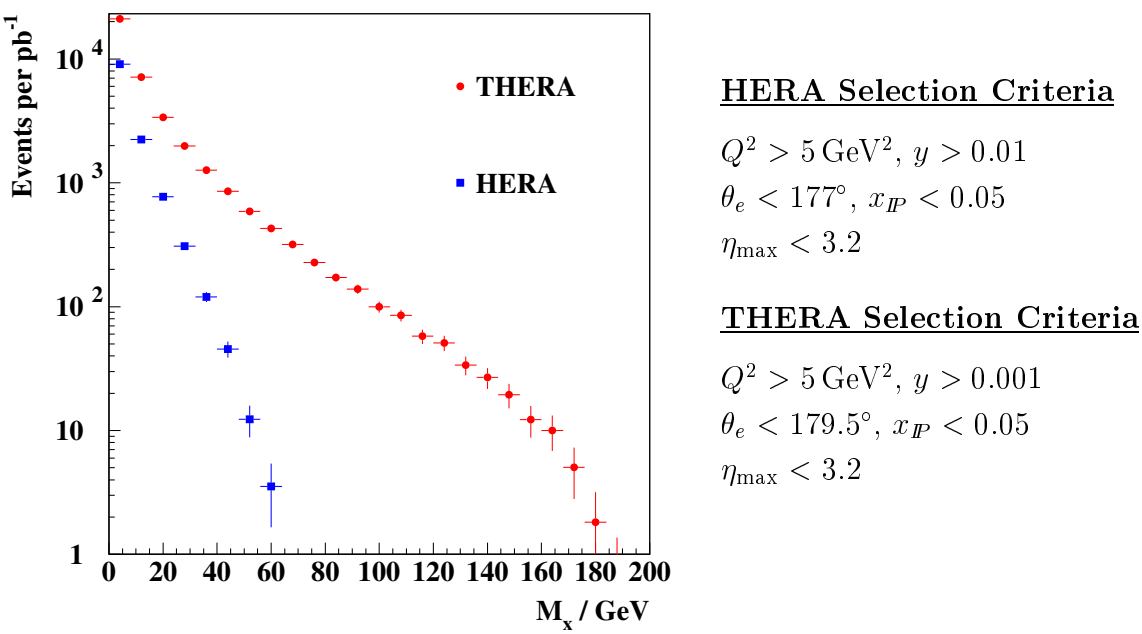

Figure 2.2.7: *Event yields per unit luminosity for the process $ep \to eXp$ after applying the quoted selection criteria at THERA (920 GeV protons, 250 GeV electrons) and HERA. The yields are shown as a function of the mass M_X and are based on an ad hoc extrapolation of a QCD fit to HERA data [44].*

of diffractive parton densities in the region of low momentum fraction. The extended range in $x_{I\!P}$ will allow an improved determination of the energy dependence of diffractive DIS from the combined HERA and THERA data. This will lead to detailed tests of the hypothesis of 'Regge' factorisation of the $x_{I\!P}$ dependence from the Q^2 and β dependences, as would be expected for a universal pomeron exchange [56].

Further tests of QCD models of diffraction and an improved understanding of the gluonic degrees of freedom are achievable by studies of hadronic final state cross sections involving additional hard scales due to the presence of charm or high-p_t jets. At HERA, the limited reach in M_X (see Fig. 2.2.5a) seriously restricts the phase space for charm and dijet production and implies that these final states can only be studied at rather large $x_{I\!P}$. As can be seen from Fig. 2.2.7, the values of M_X reached at THERA for $x_{I\!P} < 0.05$ are larger by a factor of around 3 than in the HERA case.

In diffractive events the proton can remain intact or dissociate into a low-mass hadronic system. In this sense diffractive events are directly sensitive to the conditions required to preserve the hadronic bound state. A detailed comparative study of diffractive events with and without proton dissociation could reveal information about confinement. Such an analysis can be performed if the outgoing proton beam-line is instrumented with detectors to tag the final-state protons (leading-proton spectrometer).

2.2.2 Proton structure and quantum chromodynamics

Deep-inelastic scattering has been crucial in the development of Quantum Chromodynamics since the observation of the logarithmic pattern of scaling violations in $F_2(x, Q^2)$. Over the past decades, precision measurements of structure functions and studies of final state characteristics have deepened the understanding of QCD. With the access to very low values of Bjorken x in the deep inelastic region, the exploration of extremely high Q^2 values at high luminosity, and an extension of the transverse momentum phase space, THERA promises new insights into the structure of QCD.

2.2.2.1 Perturbative QCD and structure functions

The measurements of structure functions in DIS have been accompanied by remarkable progress in QCD calculations. Both the splitting functions, to second order in α_s, and the coefficient functions, to order α_s^3, are calculated [57], and the NNLO calculation of the splitting functions is in progress. The current measurements of $F_2(x, Q^2)$ in the kinematic range of HERA are very well described by the twist-2 evolution equations, even in a range in which significant higher-twist effects and specific higher-order small-x effects were previously expected. The phenomenological success of joint determinations of the coupling constant α_s and the gluon distribution xg, together with the quark distributions, is impressive [4, 58] and has led to precise measurements of these quantities. Parton densities to NLO have been extracted over a wide kinematic range from HERA F_2 and other cross section data [59–61]. With data in the kinematic domain of THERA, both at lower x and larger Q^2, the precision of these quantities

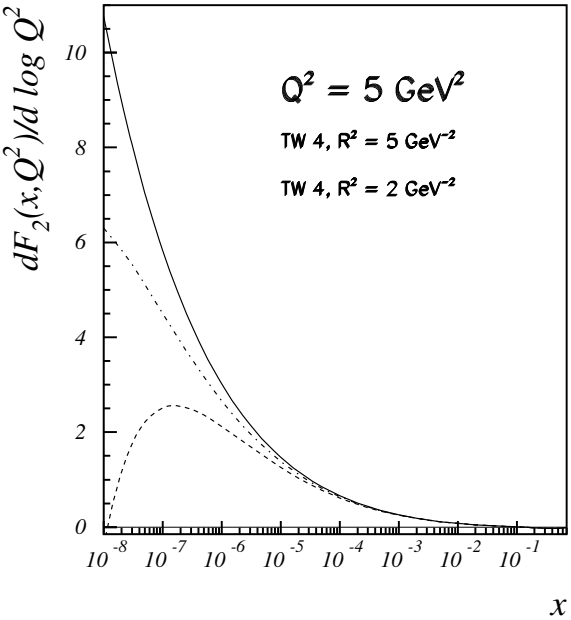

Figure 2.2.8: *The slope $\partial F_2(x,Q^2)/\partial \log Q^2$ at $Q^2 = 5\ GeV^2$ [62]. Full line: leading-order twist-2 contributions (parameterisation [61]); dash-dotted line: slope including the twist-4 contribution with a screening radius of $R^2 = 5\ GeV^{-2}$; dashed line: $R^2 = 2\ GeV^{-2}$.*

will further improve significantly (see below).

As was discussed above, an important question is how the low-x growth in F_2 as observed at HERA is tamed to satisfy the unitarity bound. Higher-order corrections to the twist-2 terms diminish the growth but do not lead to a saturation as $x \to 0$. One can expect that unitarity is restored by higher-twist contributions. First studies of these effects have been performed [62, 63] in approaches based on the light-cone expansion. Numerical results on the slope $\partial F_2/\partial \log Q^2$ for specific choices of twist-4 screening radii R are depicted in Fig. 2.2.8, showing that one may indeed probe these effects in the kinematic domain of THERA, $x \gtrsim 10^{-6}$ (see also [64]). Rather large higher twist effects [65, 66] may be seen in measurements of the longitudinal structure function F_L.

The apparent success of the complete fixed-order calculations in describing F_2 in the small-x domain is puzzling theoretically. Starting from the BFKL approximation and resumming the most singular pieces, large corrections were predicted both for the anomalous dimensions [67, 68] and for the coefficient functions [69]. Recently, large next-to-leading order resummed gluon anomalous dimensions were found [70], however with opposite sign. This led to the conclusion that they have to be stabilised by resumming even higher orders [71–73]. Formally, sub-leading terms were found to be quantitatively as important as the resummed 'leading' terms due to the strong rise of the gluon and sea quark densities in the small-x domain. This requires the knowledge of the coefficient functions also for the range of medium values of x [71, 73], where resummations are not possible. More theoretical work is needed to further develop perturbative QCD. This will be stimulated by a continuing experimental programme and data in an extended range.

Ultimately, in the regime of extremely low values of x and small Q^2, one expects that the light-cone expansion does not apply anymore. For this kinematic domain new theoretical concepts have still to be developed.

2.2.2.2 Forward jet production

In order to understand strong-interaction dynamics, inclusive cross section measurements and their interpretations have to be complemented by the investigation of the hadronic final state. At HERA, the description of details of the final states, for example in forward jet production at low x, requires to consider resolved photon structure effects in addition to the pure DGLAP evolution. However, an extension of the phase space as provided by THERA is necessary to distinguish between a DGLAP-based calculation with an additional resolved virtual photon contribution, which mimics non-k_t-ordered (i.e. non-pure-DGLAP) contributions at present energies, and small-x evolution as modelled by the BFKL [67, 68] or CCFM [74] equations. The CCFM evolution equation, based on the principle of colour coherence, is equivalent to BFKL for $x \to 0$ and reproduces the DGLAP equation for large x.

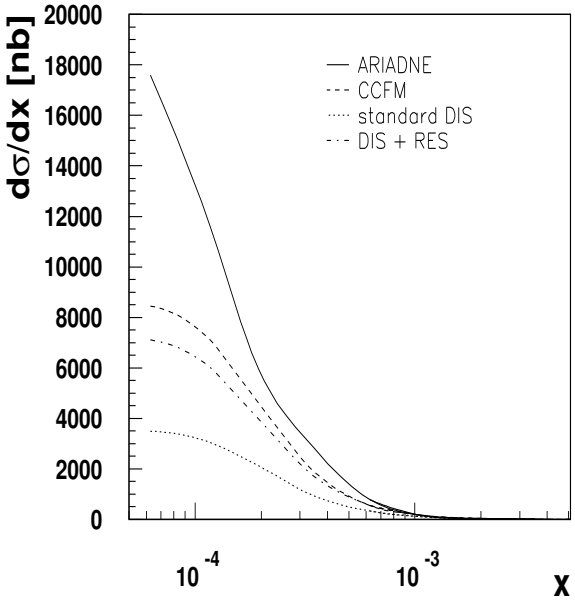

Figure 2.2.9: *Forward-jet cross section as a function of x in different models for $0.5 < p_t^2/Q^2 < 2$ and a minimum polar jet angle of $1°$. The measurements at HERA are limited to $x \gtrsim 2 \times 10^{-3}$.*

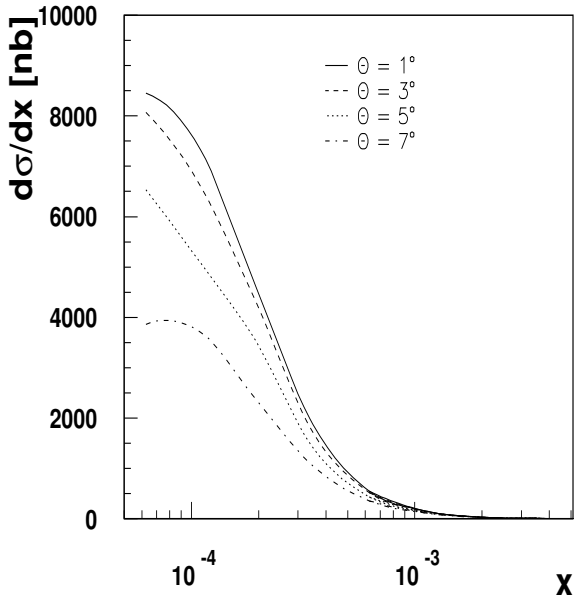

Figure 2.2.10: *Forward-jet cross section as a function of x obtained from CCFM for $0.5 < p_t^2/Q^2 < 2$, for different values of the minimum jet angle.*

At THERA the differences between these approaches become striking. In Fig. 2.2.9 the cross section for forward jet production [75] is shown as a function of x. Whereas the measurement at HERA is limited to $x \gtrsim 2 \times 10^{-3}$, the available x range at THERA is extended by one order of magnitude towards lower x. At THERA the CCFM approach predicts a much larger cross section than the model with resolved virtual photon contributions added, giving the unique opportunity to identify a new QCD regime, which can only be described by new small-x evolution equations. This not only allows us

to distinguish between the different approaches, but also to study details of the QCD cascade, which at small x includes unintegrated parton densities [48]. THERA will be the only place where these parton densities can be measured, and where the small-x parton dynamics can be clearly studied.

In Fig. 2.2.10 the forward jet cross section is shown for different minimal jet angles. On the experimental side this requires complete acceptance both in the electron and proton direction down to the lowest possible angles. From the size of the cross section $d\sigma/dx$ one would like to reach at least $\theta \sim 3°$ for the forward jet measurement, desirably even $\theta \sim 1°$. The luminosity required for such measurements is of the order of $10\,\mathrm{pb}^{-1}$.

2.2.2.3 Measurement of the strong coupling constant α_s

The accurate determination of α_s has been a central issue in many high-energy experiments which revealed a logarithmic dependence of α_s with Q^2, thereby confirming the property of asymptotic freedom of QCD (for a review see [76]). A precise measurement of this coupling constant is very important for the calculation of strong interaction processes and for unified field theories [77]. Inclusive deep inelastic scattering is particularly suitable to determine $\alpha_s(Q^2)$ because the predictions of QCD at large space-like momentum transfer can be derived in a rigorous way, based on the operator product expansion, and are free of additional assumptions like quark–hadron duality, assumptions concerning the behaviour of quark and gluon condensates, or assumptions regarding the absence or parametrisation of power corrections. The precision of QCD predictions in inclusive DIS is only limited by the present ability to evaluate perturbative corrections to sufficiently high orders. DIS measurements are therefore a unique opportunity to test QCD in a stringent way which is superior to e^+e^- annihilation and pp collisions.

Present DIS measurements of α_s [4, 58, 78] have about the accuracy of and are consistent with the world-averaged determinations of α_s. Improving these analyses is a challenge to the experimental precision and the theoretical calculations. The extension of the (x, Q^2) range and the envisaged cross section uncertainties at THERA of 1–3% lead to an estimated error [79] on $\alpha_s(M_Z^2)$ of about 0.3–0.5%, which is smaller than the current theoretical uncertainty [80] dominated by the choice of the renormalisation scale.

Reduction of the theoretical uncertainty requires the calculation of the complete 3-loop anomalous dimensions needed for NNLO QCD analyses. First results for a series of fixed moments have been obtained already [81] on the way to the complete solution. Based on these results, numerical investigations have been performed on the 3-loop splitting functions [80, 82].

Since THERA extends the Q^2 range and provides p_T values up to almost 100 GeV for jet production [83], the predictions of perturbative QCD become more reliable. Thus measurements of dijet cross sections promise to yield complementary and more accurate information on α_s and the gluon distribution than has presently been achieved at HERA [84, 85].

2.2.2.4 Heavy-flavour physics

In the last years, heavy-flavour production in ep scattering has become a subject of intense research in perturbative QCD (see [86, 87] and references therein).

Heavy quarks are produced copiously in ep collisions. The total charm and beauty cross sections at HERA are of the order of $1\,\mu$b and 10 nb, respectively. Charm production at HERA has been studied by the H1 and ZEUS collaborations in both the photoproduction and DIS regimes [10, 88, 89]. General agreement with pQCD expectations was observed in the DIS case, while a description of the charm photoproduction cross sections is more problematic for present pQCD calculations. The first measured beauty photoproduction cross sections at HERA [90] lie above the fixed-order next-to-leading order (NLO) QCD predictions [91]. No measurements of beauty production in the DIS regime at HERA have been performed so far.

An increase of the centre-of-mass energy of ep collisions from about 300 GeV at HERA to ~ 1 TeV at THERA will result in an increase of the total charm and beauty production cross sections by factors ~ 3 and ~ 5, respectively [92, 93].

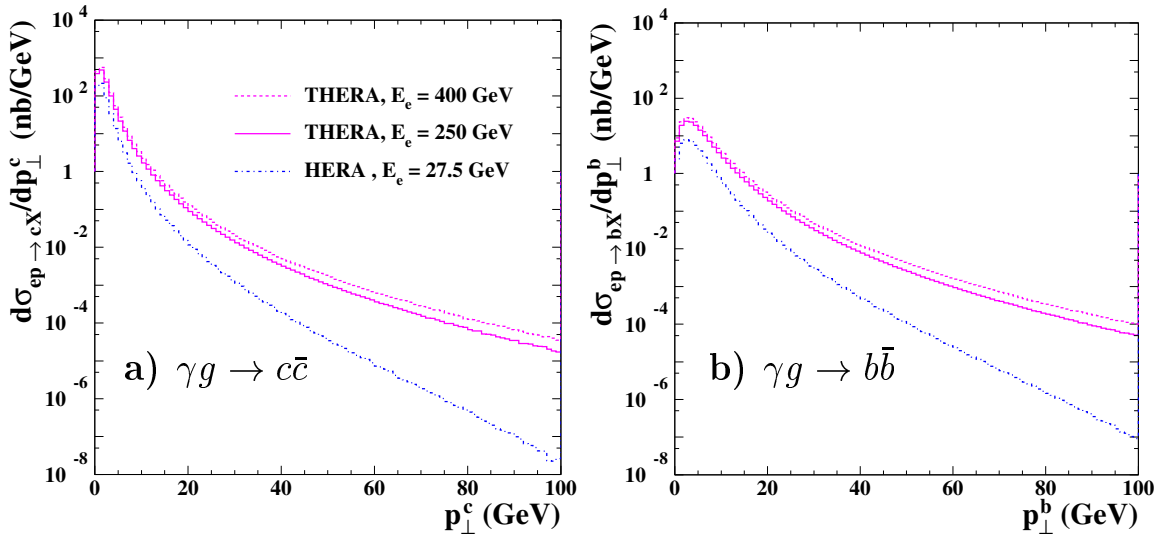

Figure 2.2.11: *The contribution of photon–gluon fusion to the differential cross sections $d\sigma/dp_\perp$ for (a) charm and (b) beauty production calculated in NLO QCD for $Q^2 < 1$ GeV^2. The solid and dashed violet curves show the predictions for THERA operation with an electron energy of 250 GeV and 400 GeV, respectively, and $E_p = 920$ GeV. The predictions for the HERA case are indicated by the dash-dotted blue curves.*

Figure 2.2.11 compares the contributions of photon–gluon fusion to the differential cross sections $d\sigma/dp_\perp^{c,b}$ ($p_\perp^{c,b}$ denoting the quark transverse momentum) at HERA and THERA, calculated within NLO QCD [91] for $Q^2 < 1$ GeV^2. The difference between the heavy quark production cross sections at THERA and HERA increases with increasing $p_\perp^{c,b}$, thereby creating the opportunity to measure charm and beauty quarks at THERA in a wider transverse momentum range. Such measurements will provide a solid basis for testing the fixed-order, resummed, and k_t-factorisation [94] pQCD calculations.

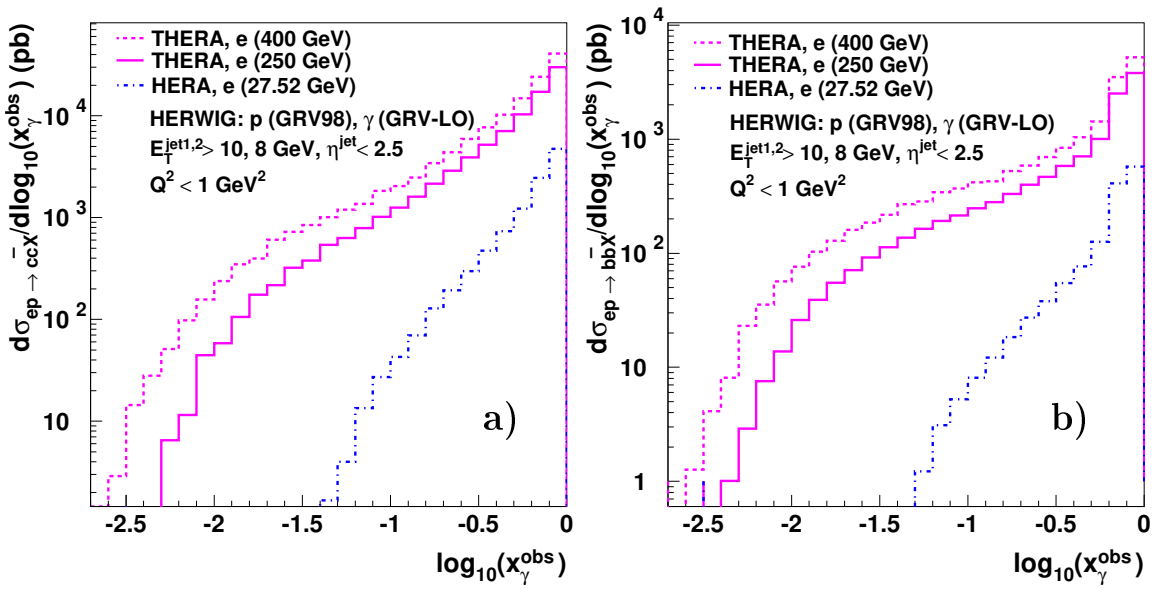

Figure 2.2.12: *The differential cross sections $d\sigma/d\log_{10} x_\gamma^{\rm obs}$ for (a) charm and (b) beauty dijet photoproduction as calculated in LO with the Monte Carlo generator HERWIG. The cross sections are shown for THERA, for a proton beam energy of* 920 *GeV and electrons with* 250 *GeV (solid magenta) and* 400 *GeV (dashed magenta), and for HERA (dashed blue).*

The reconstruction of two jets in heavy-quark photoproduction events provides an opportunity to study the gluon and heavy-quark structure of the photon [10, 88, 89]. The fraction of the photon energy contributing to the dijet photoproduction,

$$x_\gamma^{\rm obs} = \frac{\sum_{\rm jet1,2}(E_T^{\rm jet}\ e^{-\eta^{\rm jet}})}{2E_\gamma}\ , \tag{2.2.2}$$

has been found a useful observable for the investigation of the photon structure function. Here, $E_T^{\rm jet}$ and $\eta^{\rm jet}$ are the jet transverse energy and pseudorapidity, respectively, and the summation is over the two jets with highest $E_T^{\rm jet}$ within the accepted $\eta^{\rm jet}$ range. Figure 2.2.12 compares $d\sigma/d\log_{10} x_\gamma^{\rm obs}$ for charm and beauty photoproduction ($Q^2 < 1\,{\rm GeV}^2$) at HERA and THERA. The cross sections have been calculated in LO with the Monte Carlo generator HERWIG [95]. The difference between the heavy-quark dijet photoproduction cross sections at THERA and HERA increases towards smaller $x_\gamma^{\rm obs}$ values. The gluon and heavy quark structure of the photon can be studied only for $x_\gamma^{\rm obs} \gtrsim 0.1$ at HERA. The transition to the THERA energy regime will provide an opportunity to probe the structure down to at least $x_\gamma^{\rm obs} = 10^{-2}$ [92]. The gluon and heavy quark structure of the photon at THERA will be measured at rather large scale values stemming from the high E_T values of two reconstructed jets. Thus the measurements will provide complementary information to the results of future e^+e^- and $\gamma\gamma$ colliders [92].

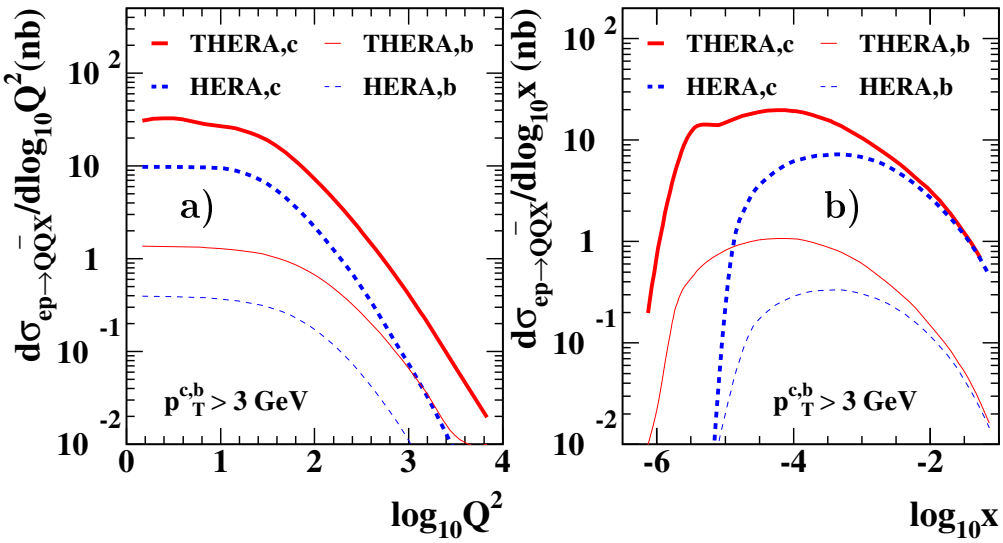

Figure 2.2.13: *The differential cross sections for charm (thick curves) and beauty (thin curves) production in neutral current DIS calculated in NLO QCD, (a) $d\sigma/d\log_{10}Q^2$ and (b) $d\sigma/d\log_{10}x$. The cross sections at THERA (solid curves) and HERA (dashed curves) are compared.*

The kinematic limits of DIS at THERA are one order of magnitude higher in Q^2 and one order smaller in x with respect to those at HERA. Figure 2.2.13 shows the differential cross sections $d\sigma/d\log_{10}Q^2$ and $d\sigma/d\log_{10}x$ for charm and beauty production in neutral current (NC) DIS calculated with the NLO code of [96]. The THERA cross sections are shifted towards smaller x values with respect to those at HERA. They are significantly above the HERA cross sections at all Q^2. Thus THERA will open new kinematic regions where the charm and beauty contributions to the proton structure function, F_2^c and F_2^b, can be extracted [93]. The measurement of charm production at large Q^2 will provide an opportunity to test the resummed pQCD calculations which treat the charm quark as a massless parton [97]. Charm production in the process of photon–gluon fusion at low Q^2 values will serve for the determination of the gluon structure of the proton in the as yet unexplored kinematic range $10^{-5} < x_g < 10^{-4}$ [93].

The theoretical description of charm production in charged current (CC) DIS is challenging [98]. The special interest in this process is caused by its sensitivity to the proton strange-quark density which is rather poorly known [99]. However, no measurement of CC charm production has been performed so far at HERA due to the small signal cross section (~ 10 pb). According to a HERWIG calculation, the cross sections for both LO CC charm production processes, $W^+s \to c$ and $W^+g \to c\bar{s}$, will be more than 6 times larger at THERA than at HERA. The differential cross sections $d\sigma/d\log_{10}Q^2$ for CC charm production are shown in Fig. 2.2.14. The THERA cross sections are shifted towards larger Q^2 with respect to those at HERA. They are one order of magnitude larger than the HERA cross sections at large Q^2 values, thereby creating the opportunity to study charm production in CC DIS at THERA [93].

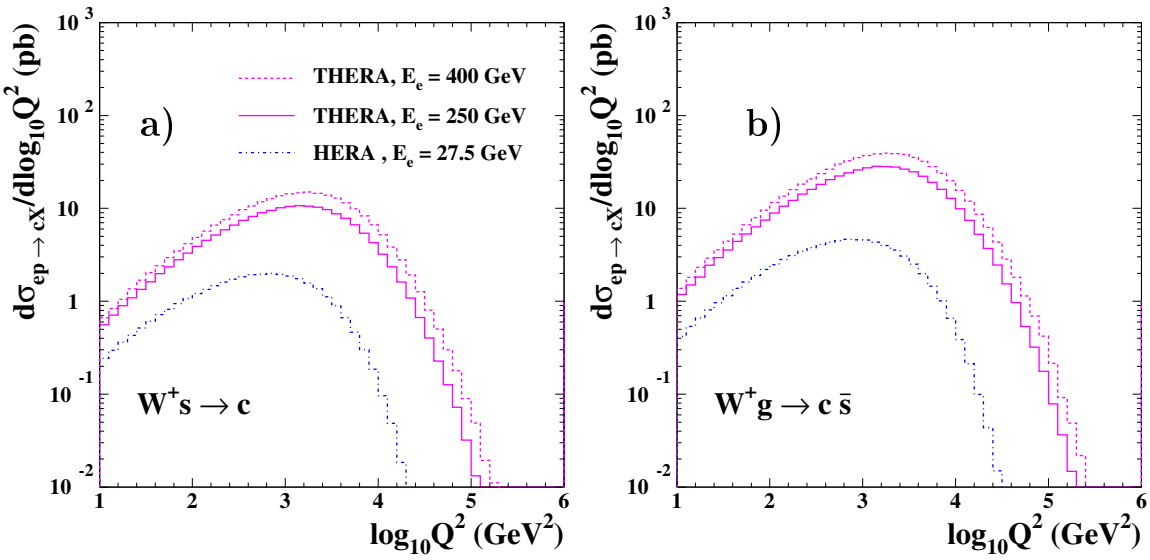

Figure 2.2.14: *The differential cross sections $d\sigma/d\log_{10} Q^2$ for charm production in charged current DIS, (a) from the strange sea and (b) from boson–gluon fusion, calculated with the LO Monte Carlo generator HERWIG. The cross sections are shown for THERA for a proton beam energy of* 920 *GeV and electrons with* 250 *GeV (solid magenta) and* 400 *GeV (dashed magenta), and for HERA (dashed blue).*

In conclusion, studies of charm and beauty production at THERA will provide unique new information about the proton and photon structures in as yet unexplored kinematic ranges.

2.2.2.5 Electroweak structure functions

In the THERA range of very high $Q^2 > M_Z^2$, the NC cross section receives comparable contributions from the exchange of photons, of Z bosons and from their interference. This is illustrated in Fig.2.2.15 showing the reduced NC cross section, $\sigma_r = \sigma_{NC}/Y_+$, defined by the relation

$$\sigma_{NC} = \frac{d^2\sigma_{NC}^{\pm}}{dx\, dQ^2}\frac{Q^4 x}{2\pi\alpha^2} = Y_+ \mathbf{F_2}^{\pm} + Y_- \mathbf{xF_3}^{\pm} \tag{2.2.3}$$

with $Y_\pm = (1 \pm (1-y)^2)$ and the fine structure constant α. Due to the Z exchange contribution, a new structure function combination $\mathbf{xF_3}$ occurs in NC [100, 101] (for a comprehensive review see [102]), which in the QPM measures a combination of the u and d valence quark distributions $q_v = q - \bar{q}$. Therefore deep inelastic NC scattering at very high Q^2 is sensitive to the quark flavours, in contrast to low Q^2, where the structure function F_2 measures only the weighted sum $\sum_q Q_q^2(q + \bar{q})$ of quark and anti-quark distributions.

Similarly, in CC scattering, the double differential cross section is given by

$$\frac{d^2\sigma^{\pm}_{CC}}{dxdy} = \frac{G_F^2}{2\pi} \cdot \left(\frac{M_W^2}{Q^2 + M_W^2}\right)^2 \cdot s \cdot \frac{1 \pm \lambda}{2} \cdot [Y_+ W_2^{\pm} \mp Y_- x W_3^{\pm}] \,, \tag{2.2.4}$$

where M_W is the CC propagator mass and G_F the Fermi constant. For a given beam charge, the cross section contains two structure functions which, in the QPM, are given by the following sums over the u- and d-type parton distributions:

$$\begin{aligned} W_2^{+(-)} &= 2x \sum (q_{d(u)} + \bar{q}_{u(d)}) \\ xW_3^{+(-)} &= 2x \sum (q_{u(d)} - \bar{q}_{d(u)}) \,. \end{aligned} \tag{2.2.5}$$

The cross section is proportional to s (which at THERA is equivalent to a beam energy of about 10^3 TeV in a neutrino fixed-target experiment). Combining NC and CC

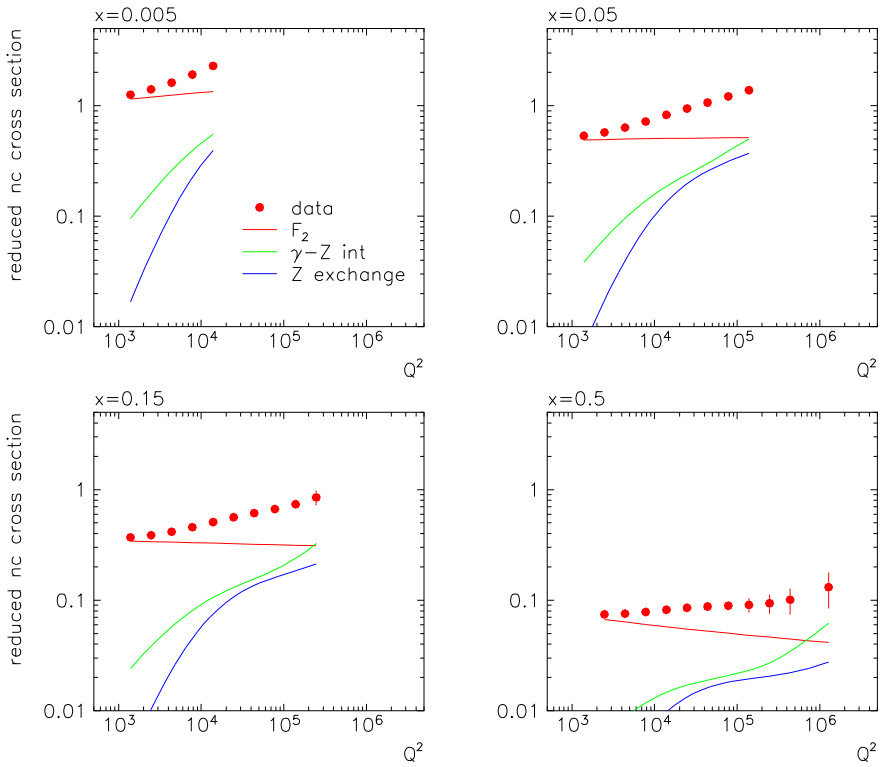

Figure 2.2.15: *Simulation of a measurement of the reduced NC DIS cross section at THERA in unpolarised electron scattering, for an integrated luminosity of* $200\,pb^{-1}$. *The error bars are a convolution of statistical and estimated systematic uncertainties. The curves represent the fraction of the one-photon exchange (red, top), of the* γZ *interference (green, middle) and of the pure* Z *exchange (blue, bottom). Towards very high* Q^2, *depending on the lepton beam charge and polarisation, the* Z *exchange contributions become increasingly important.*

$e^{\pm}p$ cross sections for different lepton polarisations, a complete unfolding [103] of the up and down quark and anti-quark distributions can be envisaged at THERA, with much higher accuracy than at HERA due to the extended Q^2 range which enhances the electroweak contributions to the cross section. The approximate symmetry of the electron and proton beam energies furthermore allows access to the up and down valence quark distributions up to very large x. This is of advantage over the standard method to access d_v at large x which relies on a comparison of proton and neutron structure functions and thus is subject to uncertain nuclear binding corrections, see [104]. The combination with the results of future high-statistics neutrino experiments [105] will permit important, flavour dependent tests of QCD.

The coverage of the full x range from about 0.005 to 1 in the region of high Q^2 at THERA is also essential for testing rigorous theoretical predictions in CC scattering [106], such as the Adler sum rule, $\int_0^1 (W_2^+ - W_2^-)dx/x = 2$, the Bjorken sum rule, $\int_0^1 (W_1^+ - W_1^-)dx = 1$, and the Gross–Llewellyn-Smith sum rule, $\int_0^1 (W_3^+ + W_3^-)dx = 6$. While the Adler sum rule holds independently of QCD, the two latter relations test QCD and are subject to higher-twist corrections which are negligible in the very high Q^2 range of THERA.

Various measurements of electroweak quantities can be performed at THERA, e.g. of the light-quark couplings, of the gauge boson masses in the space-like region and of parity violation at very high Q^2 via polarisation asymmetries in NC scattering, similarly to the pioneering experiment [107]. Utilising the high degree of lepton-beam polarisation at TESLA, one can search with much increased sensitivity for the existence of right handed currents in the new energy range which would prevent the CC cross section $\sigma^{\pm}$ from vanishing at $\lambda \to \mp 1$ (cf. eq. 2.2.4). Such a measurement at THERA for a luminosity of 100 pb^{-1} is illustrated in Fig. 2.2.16 for $\sqrt{s} = 1$ TeV.

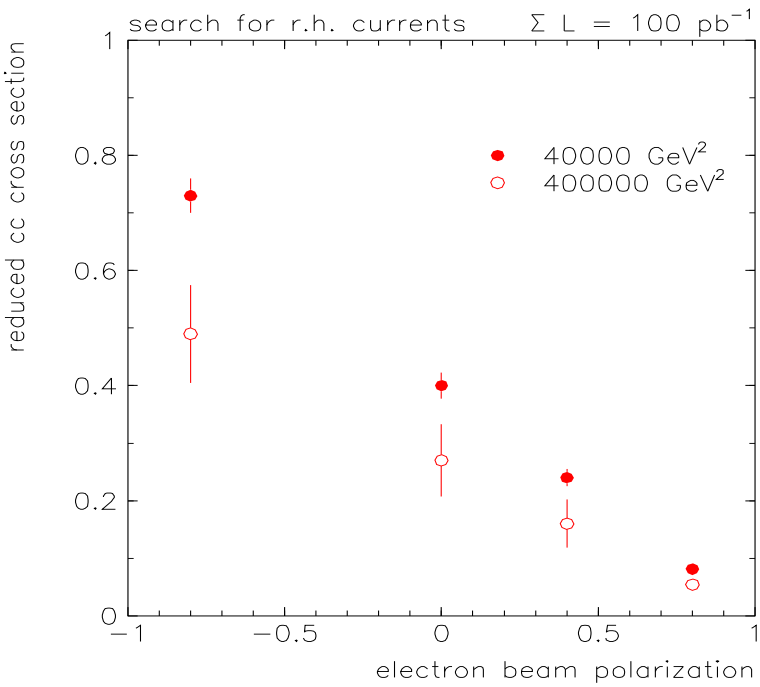

Figure 2.2.16: *Search for right-handed currents in CC scattering at THERA using a measurement of the electron–proton CC cross section as a function of the electron beam polarisation, λ. This simulation assumes a total integrated luminosity of 100 pb^{-1} distributed over four measurements at different λ.*

The extension towards the electroweak region of very high $Q^2 \sim 10^5\,\mathrm{GeV}^2$ and the coverage of the full x range make THERA an excellent facility for the exploration of the partonic nucleon structure and the test of the electroweak theory. If new interactions and particles will be found in the TeV range of energy, THERA will not only explore these but as well be crucial in accurately determining the parton distributions which have to be known for the interpretation of the new phenomena.

2.2.3 Searches for new particles or phenomena

2.2.3.1 Leptoquarks and squarks

The ep collider THERA, providing both baryonic and leptonic quantum numbers in the initial state, naturally offers the possibility to search for new bosons possessing couplings to an electron–quark pair. Such particles could be squarks in supersymmetry with R-parity violation ($\not{R}_p$), or leptoquark (LQ) bosons [108] which appear in various unifying theories beyond the Standard Model (SM).

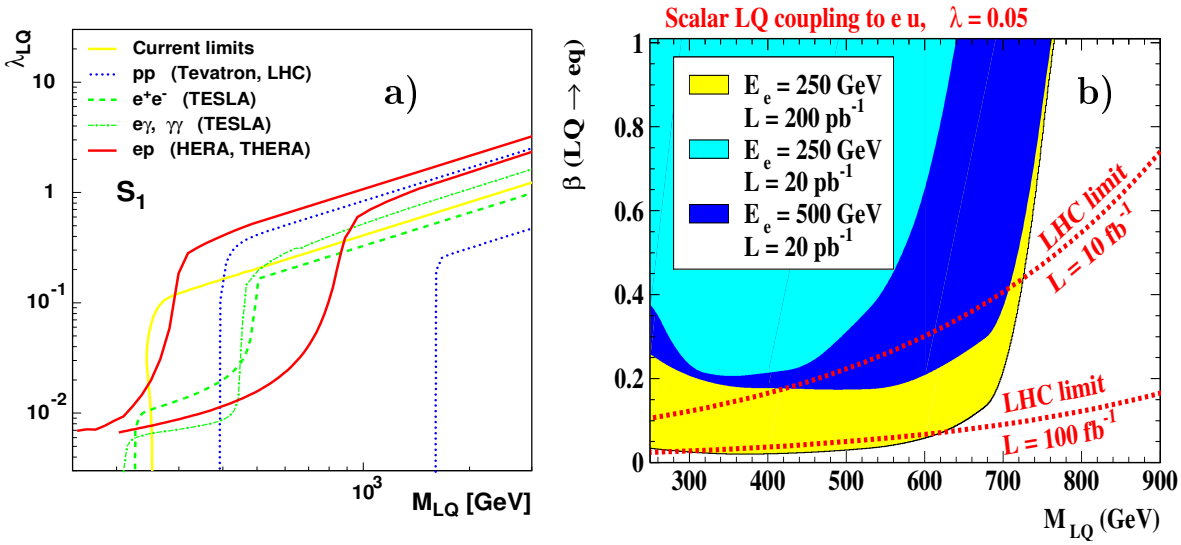

Figure 2.2.17: *(a) Mass-dependent upper bounds on the LQ coupling λ as expected at THERA (lower solid red curve, $E_e = 250\,GeV$, $E_p = 920\,GeV$, $100\,pb^{-1}$ of e^-p data), HERA (upper solid red curve, $2\times400\,pb^{-1}$ of $e^{\pm}p$ data), TESLA ($E_e = 250\,GeV$, $100\,fb^{-1}$ of ee, $e\gamma$ or $\gamma\gamma$ data), Tevatron (upper dotted curve, $10\,fb^{-1}$) and LHC (lower dotted curve, $\sqrt{s} = 14\,TeV$, $100\,fb^{-1}$). Upper limits as obtained from a global fit of various existing data sets [108] are also shown by the solid yellow curve. (b) Typical expected mass-dependent sensitivities on the branching ratio $\beta(LQ \to eq)$ of a LQ decaying to eq, at THERA for two different values of the lepton beam energy and at LHC; the coloured regions (the domains above the dashed red curves) would be probed by THERA (LHC).*

Leptoquarks (or $\not{R}_p$ squarks) with masses up to the kinematic limit, $\sqrt{s}$, could be singly produced as s-channel resonances by the fusion of the incoming electron with

a quark coming from the proton, with largest cross section when a valence quark in the proton participates in the fusion. For LQs decaying into an electron and a quark, the final state is similar to that of high-Q^2 NC DIS. For masses above the kinematic limit, LQ exchange can be parameterised by a contact interaction and could affect the measured high-Q^2 NC DIS cross section.

The sensitivity to LQs is discussed here either in the strict context of the BRW phenomenological ansatz [109], where the decay branching ratios are fixed by the model, or in the context of generic models allowing for arbitrary branching ratios.

For one of the scalar LQs described by the BRW model, with fermion number $F = 2$ (i.e. coupling to an e^- and a valence quark), the expected THERA sensitivity on the Yukawa coupling λ at the LQ-e-q vertex is illustrated in Fig. 2.2.17a as a function of the LQ mass, and compared to that of HERA-II, TESLA and hadron colliders [110]. THERA will improve the bounds expected from the full data sample of HERA by typically one order of magnitude, and its sensitivity will be significantly better than that of TESLA in the mass range 0.5–1 TeV, for a lepton beam energy of 250 GeV. However, the sensitivity of the LHC to pair-produced LQs should extend up to LQ masses of ~ 2 TeV, independently of λ. The LHC will thus probe the mass domain where resonant LQ production could be possible at THERA. This statement remains valid in 'generic' models, where the branching ratio $\beta(\mathrm{LQ} \to eq)$ of the LQ to decay into eq is not fixed but treated as a free parameter, as shown in Fig. 2.2.17b.

	$S_{0,L}$	$S_{1,L}$	$\tilde{S}_{0,R}$	$S_{0,R}$	$S_{1/2,L}$	$\tilde{S}_{1/2,L}$	$S_{1/2,R}$
$S_{0,L}$		β_ν	P_e	P_e			
$S_{1,L}$	β_ν		P_e	P_e		e^+/e^-	
$\tilde{S}_{0,R}$	P_e	P_e		P_p			
$S_{0,R}$	P_e	P_e	P_p				
$S_{1/2,L}$						P_p	P_e
$\tilde{S}_{1/2,L}$		e^+/e^-			P_p		P_e
$S_{1/2,R}$					P_e	P_e	

Table 2.2.1: *Discrimination between LQs with different quantum numbers by using the lepton beam charge (e^+/e^-) or e/p polarisation (P_e, P_p). The nomenclature of [111] has been used to label the different scalar LQ species described by the BRW model, in which the branching ratio β_ν of the LQs is known.*

If a LQ directly accessible at THERA is discovered elsewhere, THERA will be the ideal machine to disentangle the quantum numbers of this resonance and to study its properties, as illustrated in table 2.2.1: the angular distribution of the final-state lepton easily discriminates between a scalar or vector resonance; the fermion number is obtained by comparing the signal cross section in e^+p and e^-p collisions; the polarisation P_e of the lepton beam determines the chirality structure of the LQ coupling. In addition, the fact that a signal in the CC channel could also be observed provides another

discriminating variable in LQ models where the branching ratio $\beta_\nu = \beta(\mathrm{LQ} \to \nu q)$ is known. Further discrimination between LQs coupling to eu or ed would need e.g. proton beam polarisation, P_p [112].

Finally, THERA allows direct measurements of LQ couplings in the range 10^{-1}–10^{-2} for given LQ branching ratios. In contrast, pp and $p\bar{p}$ colliders are only sensitive to larger couplings via lepton-pair production induced by t-channel LQ exchange.

2.2.3.2 Contact interactions

The sensitivity of THERA to generic $eeqq$ four-fermion contact interactions (CI) has been studied in detail. Besides the exchange of very massive LQs, such CI terms can be used to parameterise any new physics process (e.g. exchange of new bosons, compositeness) appearing at an energy scale above the centre-of-mass energy. At THERA, $eeqq$ four-fermion terms would interfere (constructively or destructively) with NC DIS and thus affect the measured NC DIS Q^2 distribution. Various CI models can be considered, depending on the chiral structure of the new interaction and on the flavours of the involved quarks. CI models which violate parity are already severely constrained by the precise measurements of atomic parity violation. For models conserving parity, scales up to ~ 18 TeV could be probed at THERA, extending considerably beyond the existing bounds. The LHC collider should be able to probe even larger scales. However, should an $eeqq$ CI be within its reach, THERA would give deeper insights on the chiral structure of this new interaction by exploiting the lepton beam polarisation. For general CI models involving all possible flavour and chiral structures, searches at THERA and LHC will be to a large extent complementary.

2.2.3.3 Large extra dimensions

The t-channel exchange of Kaluza–Klein gravitons in models with large extra dimensions [113] would also affect the Q^2 distribution of the observed NC DIS events. Compactification scales up to ~ 2.8 TeV could be probed at THERA. However, the existence of extra dimensions corresponding to much larger scales should be detected by the analysis of dijet events at the LHC. It has been conjectured that fermions with different gauge quantum numbers are localised on different 'branes' in the full space-time [114]. For accessible compactification scales, relevant and complementary information on this fermion localisation could be provided by TESLA and THERA, in contrast to the LHC, where the two-gluon initial state would dominate the cross section.

2.2.3.4 Excited leptons

The single production of excited leptons (electrons, e^*, and neutrinos, ν^*) at THERA can proceed via the t-channel exchange of a gauge boson. Assuming an equal coupling, f, of the e^*e pair to $U(1)$ and $SU(2)$ bosons, the expected sensitivity to f/Λ has been studied as a function of the e^* mass M_{e^*} (here Λ denotes the compositeness scale [115]). For $f/\Lambda = 1/M_{e^*}$, excited electrons could be detected up to masses of ~ 1 TeV at THERA with a luminosity of $200\,\mathrm{pb}^{-1}$ and beam energies of 800 GeV.

A similar sensitivity is expected for excited neutrinos. This extends far beyond the current bounds of HERA and LEP. Pair production of e^* and ν^* at the LHC should probe this mass domain independently of the unknown couplings.

2.2.4 Resolving the partonic structure of the photon

In high-energy processes, the photon exhibits a "hadronic structure". At low Bjorken x, the photon structure function $F_2^\gamma(x, \hat{Q}^2)$ is expected to behave like the proton F_2, i.e. to increase towards lower x at sufficiently large $\hat{Q}^2$, where $\hat{Q}^2$ is the scale used to probe the quasi-real photon. Unique expectations for the photon are the logarithmic rise of the hadronic structure function with the scale, $\hat{Q}^2$, and a large quark density at large x. Observations of these phenomena are basic tests of QCD and essential to understanding the structure of the photon.

The ep collider THERA offers the opportunity to study the partonic structure of the photon in terms of the variable x_γ, which measures the fraction of the photon momentum participating in the hard interaction. At lowest order, x_γ is equal to unity for 'direct process' (Fig. 2.2.18a), whereas 'resolved processes' (Fig. 2.2.18b) are characterised by a smaller x_γ. THERA extends the kinematic range in x_γ by approximately one order of magnitude towards smaller values with respect to existing colliders (HERA and LEP) and significantly increases the accessible hard scale $\hat{Q}^2 = p_T^2$, i.e. the square of the parton transverse momenta (corresponding to Q^2 in deep inelastic $e\gamma$ scattering).

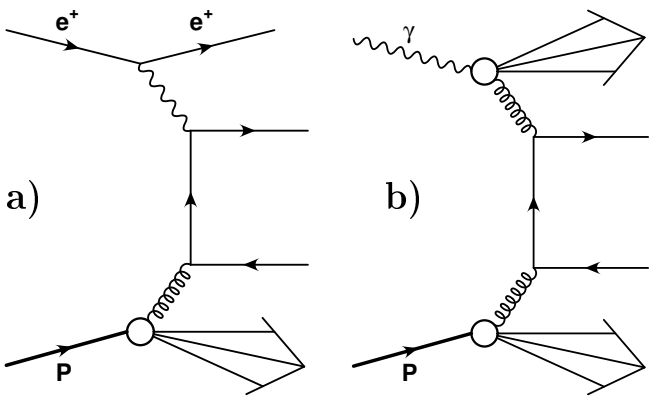

Figure 2.2.18: *Examples of LO (a) direct photon and (b) resolved photon processes in ep collisions.*

Photoproduction ($Q^2 < 1\,\mathrm{GeV}^2$) of particles (hadrons or prompt photons) or jets at high transverse momenta provides information on the gluonic content of the quasi-real photon (Fig. 2.2.18b), complementary to that from deep inelastic $e\gamma$ scattering. The photoproduction of dijets, heavy quarks and prompt photons has been studied [92, 116, 117], with the emphasis on the potential of THERA to yield information on the structure of the real photon. The possibility of measuring the structure of the virtual photon at THERA has also been considered [118]. In addition, it has been demonstrated that a first determination of the spin structure of the photon at THERA appears feasible for luminosities significantly exceeding $\mathcal{O}(10\,\mathrm{pb}^{-1})$ [119].

Good knowledge of the hadronic interactions of the photon is important for future

high energy physics investigations, e.g. for determining the Standard Model background in searches for new particles. The present situation is not satisfactory, as data for some processes, such as photoproduction of dijets at HERA, are not in agreement with existing NLO QCD calculations [120, 121]. The level of agreement for processes involving resolved virtual photons is even more problematic.

2.2.4.1 Kinematics and comparison with other colliders

A first estimate of the benefits of THERA can be obtained by comparing the kinematic reach of THERA ($\sqrt{s} \approx 1\,\mathrm{TeV}$) with that of LEP ($\sqrt{s} \approx 200\,\mathrm{GeV}$), HERA ($\sqrt{s} \approx 300\,\mathrm{GeV}$) and a future linear e^+e^- collider, TESLA, ($\sqrt{s} \approx 500\,\mathrm{GeV}$). Of interest for this section are the minimal accessible x_γ,

$$x_\gamma^{\min}\Big|_{e^+e^-} = \frac{p_T e^{\pm\eta_{\mathrm{CM}}}}{2E_e - p_T e^{\mp\eta_{\mathrm{CM}}}}\,, \qquad x_\gamma^{\min}\Big|_{ep} = \frac{E_p p_T e^{-\eta_{\mathrm{LAB}}}}{2E_e E_p - E_e p_T e^{\eta_{\mathrm{LAB}}}}\,, \tag{2.2.6}$$

the range of the hard scale, $\hat{Q}^2$, and the pseudorapidity, η, of the jets in resolved-photon events which determines the geometrical acceptance of the detector.

In Fig. 2.2.19a, the minimum photon momentum fraction, $x_\gamma^{\min}$, for a fixed transverse momentum of $p_T = 10\,\mathrm{GeV}$, is shown as a function of the laboratory-frame pseudorapidity for e^+e^- and ep colliders. It can be seen that for a given η, THERA accesses $x_\gamma^{\min}$ values that are an order of magnitude smaller than at HERA. The minimum x_γ at TESLA would also be beyond the reach of LEP and HERA. However, smaller values of x_γ can be accessed at THERA than at TESLA in the very forward direction ($\eta_{\mathrm{LAB}}^{ep} > 2$), reaching a minimum for the given transverse momentum at $\eta_{\mathrm{LAB}}^{ep} \approx 4.6$. This demonstrates the need for an instrumentation of the very forward direction at THERA which allows an accurate measurement of jets up to the rapidities discussed here.

The accessible regions in $\hat{Q}^2$ and x or x_γ are shown in Fig. 2.2.19b, taking into account restrictions imposed by limited detector acceptance. Typical kinematic selection criteria are imposed, as indicated in Fig. 2.2.19b for LEP and HERA. The same cuts have also been applied for the TESLA and THERA studies, although it is hoped that the future experiments would have improved acceptance in the very forward and backward regions. Although the e^+e^- machines will yield the lowest values of x, the ep machines can probe smaller values of x_γ for a given $\hat{Q}^2$. In particular, THERA will provide valuable additional information on the structure of the photon down to $x_\gamma \sim 0.01$ at high p_T, thus complementing TESLA and the current experiments.

2.2.4.2 Jet production

Inclusive dijet and charm production at THERA have been studied and compared with what is currently achievable at HERA [92, 116, 122]. Heavy quark production at THERA is discussed in Sect. 2.2.2.4. Here the focus is on the potential of the THERA collider in testing the partonic content of the photon using jets and heavy quarks as tools. In dijet production, the observable x_γ^{obs}, defined as the fraction of the photon

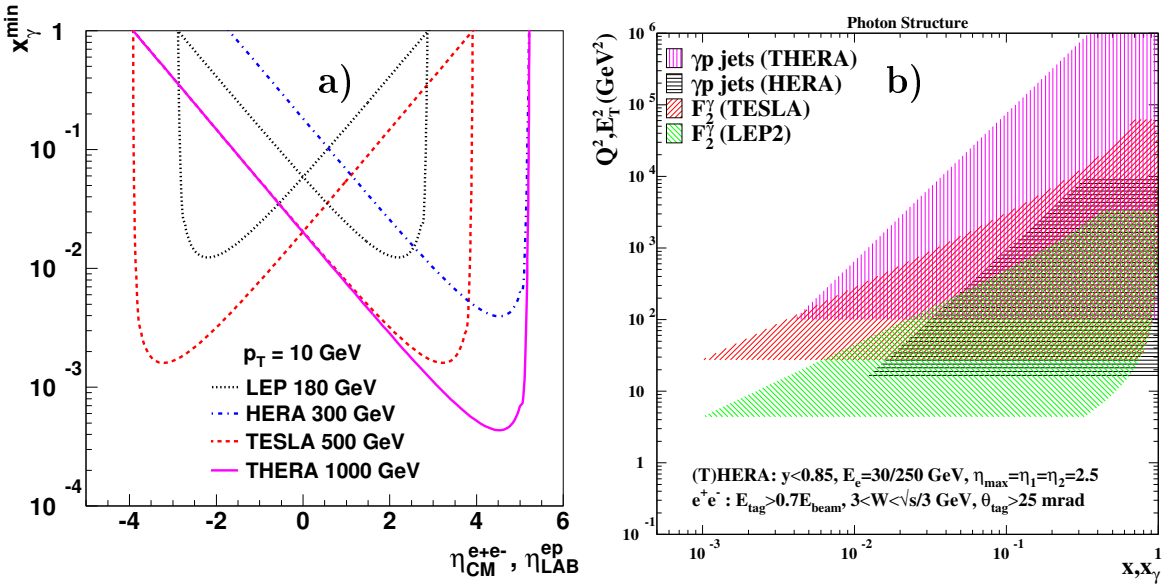

Figure 2.2.19: *(a) The minimum photon momentum fraction, $x_\gamma^{\min}$, as a function of the rapidity in the centre-of-mass frame for e^+e^- colliders and in the laboratory frame for ep colliders. (b) Range in $\hat{Q}^2$ (Q^2 or p_T^2) versus x or x_γ with kinematic cuts reflecting a realistic detector acceptance (indicated at the bottom of the figure). The kinematic reach of THERA is compared with that of TESLA, HERA and LEP2.*

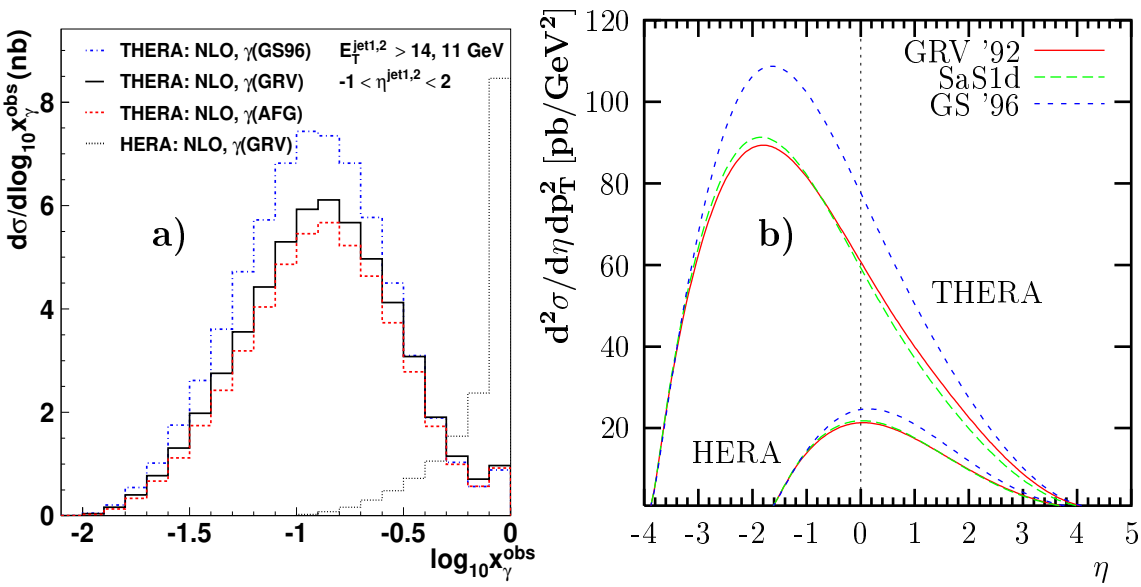

Figure 2.2.20: *(a) The differential cross section, $d\sigma/d\log_{10} x_\gamma^{\rm obs}$, for inclusive dijet photoproduction at HERA and THERA as predicted by a NLO calculation. (b) The differential cross section for photoproduction of charm in ep reactions, $ep \to e\, c\bar{c}\, X$, at $p_T = 10$ GeV calculated in LO in the massless (VFNS) scheme.*

energy producing the two jets of highest transverse energy (see eq. 2.2.2), is used as an estimator for x_γ [123]. The cross section $d\sigma/d\log_{10} x_\gamma^{\rm obs}$ in NLO [124, 125] is shown in Fig. 2.2.20a. It can be seen that the prediction for HERA is strongly peaked at $x_\gamma^{\rm obs}$ close to unity, whereas the predictions for THERA peak at $x_\gamma^{\rm obs} \sim 0.1$. Differences of up to 50% between the results for different structure function sets [126–130] are observed. The charm cross section $d^2\sigma/d\eta dp_T^2$ from a LO calculation for $p_T = 10$ GeV is peaked at $\eta \approx 0$ for HERA and at $\eta \approx -2$ for THERA (see Fig. 2.2.20b). The cross section maximum at THERA is enhanced by a factor of about 5 as compared to HERA. Again, some sensitivity to the choice of the photon parton parametrisation is evident. For THERA, the cross section ratio of resolved to direct photoproduction of charm exceeds unity at $\eta > -3.5$ and rapidly increases with growing η (see Fig. 2.2.21).

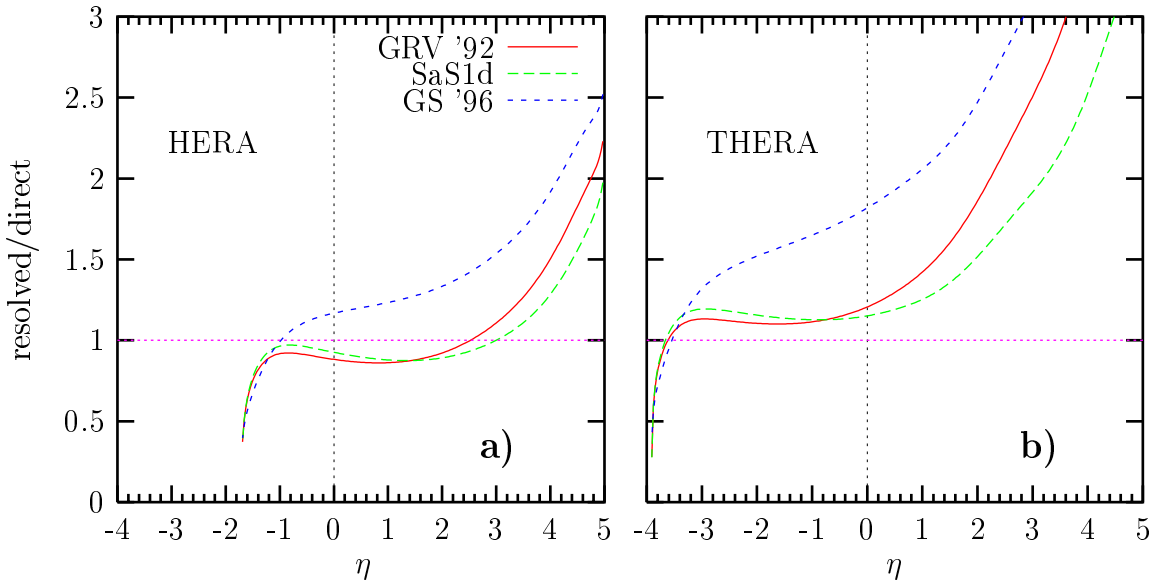

Figure 2.2.21: *The ratio of the resolved to the direct contributions to the charm photoproduction cross sections $d^2\sigma/d\eta dp_T^2$ in ep reactions at $p_T = 10$ GeV, (a) for HERA and (b) for THERA. The cross sections have been calculated to LO in the massless (VFNS) scheme, using the CTEQ5L parton distribution set for the proton and three different LO parton distribution sets for the photon.*

2.2.4.3 Prompt photon production

Prompt photon photoproduction, $ep \to \gamma X$ (the deep inelastic Compton scattering process), allows the photon structure to be studied in yet another way [117]. For example, calculations demonstrate that in the forward region ($\eta_\gamma > 0$) the Compton process is dominated by the reaction ($gq \to \gamma q$) with a cross section nearly ten times larger than at HERA and extending to larger transverse momenta of the photon. Thus prompt photon production will allow the gluonic content of the photon to be probed.

2.3 Experimentation at THERA

2.3.1 Collision of TESLA electrons with HERA protons

The achievable luminosity for THERA, the TESLA–HERA electron proton collider, is constrained by the electron beam power, the intra-beam scattering which limits the emittance of the proton beam, and the β-function of the protons which is achievable within the practical limits of focusing at the interaction point (IP). In the limit of ultra-short bunches and assuming head-on collisions, round beams, and equal transverse beam sizes for electrons and protons at the crossing point, the luminosity L is given by

$$L = \frac{N_e N_p f_b \gamma_p}{4\pi\varepsilon_p \beta^*} \ , \tag{2.3.1}$$

where ε_p is the normalised proton beam emittance or mean square beam size divided by the betatron parameter β^*, N_e and N_p are the numbers of electrons and protons per bunch, f_b is the collision frequency, and γ_p is the proton Lorentz factor. Once the energy of the electron beam is chosen, the total electron beam current ($I_e = N_e \cdot e \cdot f_b$) is limited by the allowed electron beam power or $I_e = e \cdot P_e/E_e$. The luminosity L is independent of the bunch charge N_e and the collision frequency f_b as long as their product, expressed by the beam power P_e, is constant. The luminosity can thus be written in the following form:

$$L = 4.8 \times 10^{30}\,\mathrm{cm}^{-2}\,\mathrm{s}^{-1} \cdot \frac{N_p}{10^{11}} \frac{10^{-6}\,\mathrm{m}}{\varepsilon_p} \frac{\gamma_p}{1066} \frac{10\,\mathrm{cm}}{\beta^*} \frac{P_e}{22.6\,\mathrm{MW}} \frac{250\,\mathrm{GeV}}{E_e} \ . \tag{2.3.2}$$

2.3.1.1 Proton phase space density

The ratio N_p/ε_p is called beam brightness. In conjunction with a certain bunch length and energy spread of the protons it is a measure of the phase space density. The beam brightness is limited by space charge forces in the low-energy part of the accelerator chain. But also at high energy, the beam brightness is subject to slow decay due to Coulomb scattering of protons within the bunch, the so-called intra-beam scattering (IBS) [131], which, in the presence of dispersion, leads to emittance growth. The limitation of beam brightness depends on the longitudinal charge density and thus on the bunch length σ_p. This is, however, also a critical parameter at collision since it limits the effective size of the proton beam at the IP. For long bunches (large σ_p compared to β^*), collisions occur at significantly increased cross sections due to the quadratic increase of β as a function of the distance s from the IP (hourglass effect). In addition, the finite bunch length reduces the effective proton beam cross section in case of a crossing angle. For given radio-frequency (RF) focusing forces, the bunch length is given by the longitudinal emittance, which is also subject to limitation by space charge effects at low energy and to slow growth due to IBS at high energy. Due to practical limitations of the RF focusing system and dynamical stability considerations, there is only a limited range for optimising the bunch length within these constraints. At low energy, one wants to maximise the bunch length to achieve maximum brightness. At

high energies, at collisions, one wants minimum bunch length to achieve the minimum effective beam cross section.

Taking these general limitations into account, an IBS growth time of 2.9 hours results for a 1 TeV proton beam in HERA with an initial transverse normalised emittance of $\varepsilon_p = 1 \times 10^{-6}$ m, an initial bunch length of $\sigma_p = 10$ cm, and an initial relative energy spread of $\sigma_{p\epsilon} = 1.1 \times 10^{-4}$. The longitudinal growth time is just 2 hours. This determines the luminosity lifetime and must be considered as an upper limit for the proton density. In order to achieve smaller proton beam emittance, emittance cooling is required. For example, to reduce the emittance by a factor of five, cooling times of 12 min must be achieved to balance the IBS emittance growth. Up to this point, no such powerful cooling systems are available. This leads to the conclusion, that a proton beam normalised emittance in the order of $\varepsilon_p = 1 \times 10^{-6}$ m with $N_p = 10^{11}$ has to be considered as a minimum for HERA. It represents quite a challenge to achieve the corresponding beam brightness in the injector chain. At present, the best beam brightness values achieved in the DESY III synchrotron are in the range of $N_p/\varepsilon_p = 1.3 \times 10^{11}/3 \times 10^{-6}$ m [132] which falls short by a factor of 2.3 to the target value of $10^{11}/10^{-6}$ m. Electron cooling in the lower energy stages [133] may be necessary to achieve the target value. Active feedback to damp injection oscillations might be needed in the higher energy stages. The conclusion is that the target values of $N_p = 10^{11}$, $\varepsilon_p = 10^{-6}$ m, $\sigma_p = 16$ cm and $\sigma_{p\epsilon} = 1.1 \times 10^{-4}$ constitute an ambitious but maybe not unrealistic goal for the phase space density of an LC–ring electron–proton collider at HERA.

2.3.1.2 Interaction region layout

Small values of the β-function β^* at the IP are essential for high luminosity. The β-function is limited by the chromaticity of the protons which is generated in the low-β quadrupole magnets, by aperture limitations in connection with a maximum achievable field gradient in the quadrupole magnets and by the proton bunch length. As chromaticity and maximum beam size grow linearly with the final focus quadrupole distance from the IP, for fixed β^*, it is desirable to focus electrons and protons simultaneously, thereby minimising the distance of the quadrupole magnets to the IP. At 1 TeV proton energy, the bunch length should be 10 cm or longer for adequate IBS life times. In addition, in order to avoid the excitation of synchro-betatron resonances of the protons by the electrons the crossing angle must be limited to a few mrad. This is supported by recent tracking calculations [134]. Additional beam separation technique is thus required, possibly using soft magnetic separation.

Figure 2.3.1 shows a component layout and the resulting envelope functions that meet the requirements. The layout has been designed for a ratio of proton to electron energies of 1 TeV/300 GeV and is taken from previous work on electron–proton colliders based on a LC–ring combination [135]. The electron beam is focused by a superconducting quadrupole triplet which is placed at 5 m from the IP and two doublets which give a β^* of 97 cm at the IP and also low β at 25 m and 50 m from the IP. At these latter positions strong quadrupoles for the protons are placed which, because of the low

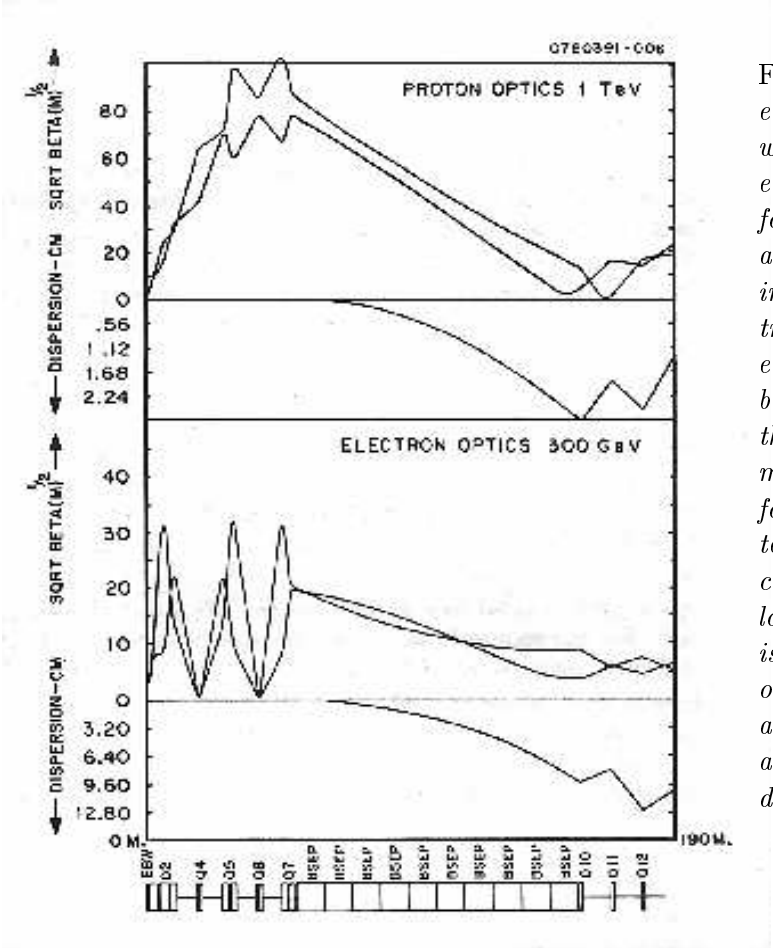

Figure 2.3.1: *Possible layout for an electron–proton interaction region, which works for proton/electron energy ratios between one and four. The case for* 1 *TeV protons and* 300 *GeV electrons as presented in [135] is shown. One quadrupole triplet and two doublets focus the electron beam strongly. At the beam envelope waists in between these lenses, strong quadrupole magnets are placed which help to focus primarily the protons. After the two beams are properly focused, at* 70 *m from the IP, a long soft quadrupole magnet, which is aligned along the electron beam orbit, smoothly bends the protons away. This arrangement avoids any extra upstream synchrotron radiation by the beam separation.*

electron β there, have minimum influence on the electrons while effecting a β^* of 10 cm for the protons. The quadrupole gradients are 150 T/m, the lengths of the quadrupoles vary between 2 and 4 m to achieve a good optical match. An aperture of 30 mm appears to be technically feasible but very challenging since it requires peak fields of 9 T. The beta function of the protons reach values of 1000 m at the maximum in the low-beta quadrupoles. This corresponds to ten standard deviations of the proton beam size and appears to be acceptable based on HERA operational experience. A 100 m long separator magnet, which is placed at 60 m distance from the IP, acts to separate the two beams. It is a soft, defocusing quadrupole ($G = 10$ T/m) which is aligned along the electron orbit while the protons pass off-centre and receive a deflection. A tiny crossing angle of 0.05 mrad avoids the first parasitic crossing at 65 m and provides the required small initial pre-separation of the two beams. This arrangement avoids any extra upstream synchrotron radiation by the beam separation magnets. It is remarkable, that this scheme is very flexible as far as the energy ratio of the beams is concerned. It allows to separate beams with a ratio of beam energies between one and four.

The electron beam is focused by the beam–beam interaction at the IP as well as the outgoing lenses. Inclusion of the beam–beam interaction in the linear optics shows that the e-beam is still well behaved on its way out. Full separation is achieved at 50 m from the IP.

The trajectory of the TESLA beam line is planned to be tangential to the HERA Straight Section West. The beam separation scheme is designed such that no bends in the electron beam lines are necessary for the incoming electron beam. However, the outgoing protons receive a kick of 14 mrad and a radial displacement of 468 mm. This could be compensated by disabling the first superconducting dipole magnet for the outgoing protons, accompanied by a small correction kick of 1 mrad and a radial shift of the IP by approximately 524 mm away from the centre of the ring. The final geometry of the TESLA tunnel and beam line should take this into account. The outgoing electrons are allowed to receive a bending angle which would shorten the separation section on the other side considerably. The additional space made available in this way is needed to restore the proton orbit for incoming protons, making use of the now available dipole magnet from the other side. A complete layout of the geometry has not yet been designed.

2.3.1.3 Luminosity estimate

In Table 2.3.1, the parameters of an (e-LC)-(p-ring) collider based on TESLA and HERA parameters are summarised. In calculating the luminosity, the limitations in β and proton beam brightness as discussed in the previous sections as well as the hourglass effect and the effect of a crossing angle have been taken into account. Assuming a bunch length of 10 cm to be possible, the hourglass reduction factor is 0.9. Even a tiny crossing angle of $\theta = 0.05$ mrad changes the cross section and thus the luminosity by 6%. Combining all these numbers yields a luminosity of $L = 4.1 \times 10^{30}\,\mathrm{cm}^{-2}\,\mathrm{s}^{-1}$ when operating TESLA at $E_e = 250$ GeV and HERA at $E_p = 1$ TeV. In a year of running this luminosity corresponds to about $40\,\mathrm{pb}^{-1}$ assuming an efficiency of 60% and 200 days of operation.

If THERA is operated with equal electron and proton energies, the focusing could be made much more efficient. Such an energy setting is not favourable for low x physics because the electron would be scattered even closer to the electron beam direction than in the asymmetric energy case. This constraint, however, is not important for high-Q^2 studies, for which, on the other hand, maximising the luminosity is of utmost importance.

With equal beam energies, a single low-beta doublet could be used to focus the beam to beta functions as small as 1 cm. The superconducting quadrupole magnets need to have a length of $l = 3$ m, and would be placed starting at 2 m from the IP. An aperture of 20 mm would correspond to 10 times the r.m.s. beam size in these magnets. A peak field of 5 T would be required to produce the gradients needed in this setup. The magnet cryostat would have an estimated outer diameter of 40 cm. The detector would have to provide space for these magnets by giving up small-angle detector acceptance. The strong hourglass effect in this situation, with 16 cm bunch length and 1 cm beta function, must be overcome following a proposal by Dohlus and Brinkmann [136] which features a moving β-waist around the IP due to time-dependent focusing by introduction of RF quadrupoles. This way, the minimum β-function occurs at the location and time where the e-beam collides with a slice of the proton beam

electron beam parameters	
electron energy	$E_e = 250\,\mathrm{GeV}$
number of electrons per bunch	$N_e = 2 \times 10^{10}$
bunch length	$\sigma_{se} = 0.3\,\mathrm{mm}$
invariant emittance	$\varepsilon = 100 \times 10^{-6}\,\mathrm{m}$
beta function at IP	$\beta_{x,y} = 0.5\,\mathrm{m}$
electron tune shift	$\Delta\nu_y = 0.228$
disruption	$D = 0.02$
bunch spacing	$t_{be} = t_{bp} = 211.37\,\mathrm{ns}$
RF frequency	$f = 1301\,\mathrm{MHz}$
accelerating gradient	$g = 23.4\,\mathrm{MV/m}$
beam pulse length	$T_p = 1.19\,\mathrm{ms}$
number of bunches	$56 \times (94 + 6$ empty bunches$)$
duty cycle	$d = 0.5\%$
repetition rate	$f_r = 5\,\mathrm{Hz}$
beam power	$P_b = 22.6\,\mathrm{MW}$
proton beam parameters	
proton energy	$E_p = 1\,\mathrm{TeV}$
number of protons per bunch	$N_p = 10^{11}$
number of bunches	$N_{pb} = 94$
beam current	$I_p = 71\,\mathrm{mA}$
bunch length	$\sigma_p = 10\,\mathrm{cm}$
beta functions at IP	$\beta^*_{xp} = 10\,\mathrm{cm}$
normalised emittance	$\varepsilon_p = 1 \times 10^{-6}\,\mathrm{m}$
IBS growth time transv./long.	$\tau_s = 2.88\,\mathrm{h}, \tau_x = 2.0\,\mathrm{h}$
collider parameters	
hourglass reduction factor	$R = 0.9$
crossing angle	$\theta = 0.05\,\mathrm{mrad}$
luminosity	$L = 4.1 \times 10^{30}\,\mathrm{cm}^{-2}\,\mathrm{s}^{-1}$

Table 2.3.1: *Main parameters of an electron–proton collider based on HERA and TESLA.*

and the beam size remains uniform during the whole collision time. In the horizontal plane, the beam size would be dominated by the crossing angle and the β-function can be relaxed to 3 cm. The luminosity which can be achieved in this scenario is estimated to be $L = 2.5 \times 10^{31}\,\mathrm{cm}^{-2}\,\mathrm{s}^{-1}$ for $E_e = E_p = 500\,\mathrm{GeV}$. This scenario uses both arms of TESLA, which is possible due to the standing-wave type cavities in the superconducting LC. With the TESLA machine upgraded in power, energies as high as 400 GeV per arm are envisaged, which for THERA opens the possibility to run at $E_e = E_p = 800\,\mathrm{GeV}$. This provides a maximum energy in ep scattering of $\sqrt{s} = 1.6\,\mathrm{TeV}$ at an estimated luminosity of $1.6 \times 10^{31}\,\mathrm{cm}^{-2}\,\mathrm{s}^{-1}$. Thus with equal beam energies and a dynamic focusing system, integrated luminosities of about $200\,\mathrm{pb}^{-1}$ per year are in reach for THERA.

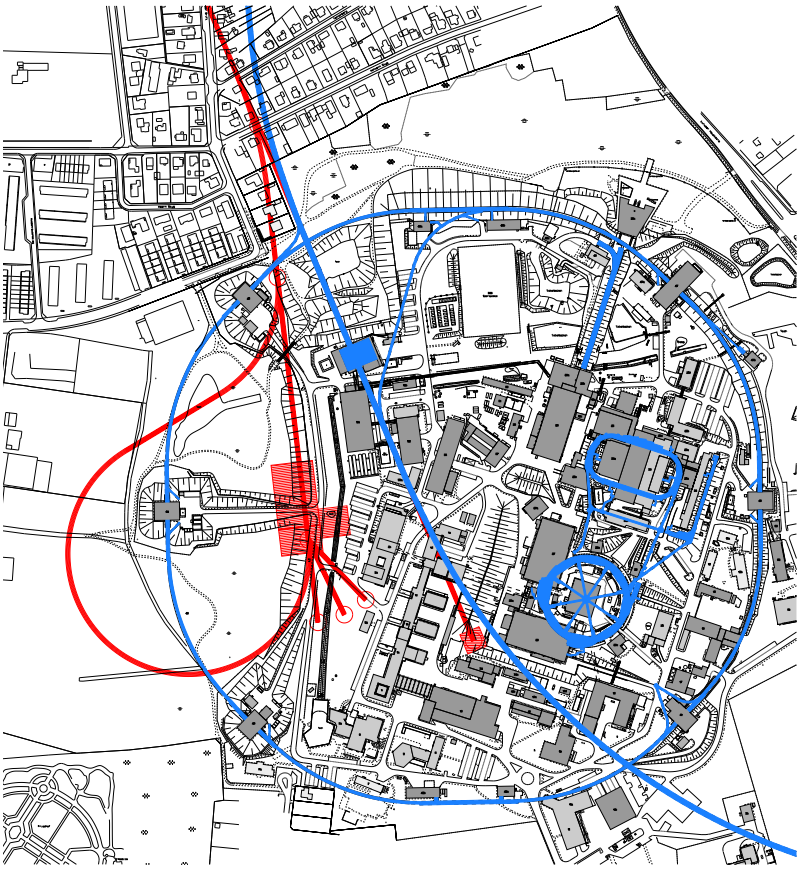

Figure 2.3.2: *Site of THERA: TESLA (red) is foreseen to be built tangentially to the HERA ring (blue) such that electrons from North hit protons in the West Hall on the DESY site. The PETRA ring is seen which serves as a pre-accelerator for HERA protons. The PETRA lepton injection line will be instrumented with superconducting magnets to arrange protons travelling clockwise in HERA. After collision the TESLA electrons will be dumped on site.*

2.3.1.4 Auxiliary systems

The THERA accelerator site at DESY is shown in Fig. 2.3.2. Electrons or positrons are injected at the far North end into the linac and accelerated up to full energy. A dedicated THERA electron gun and a short injector unit will be necessary. In order to operate the *ep* collider, the protons have to travel clockwise around HERA. For injecting the proton beam, the current lepton injection line has to be used, whose strong bends require superconducting magnets for a 40 GeV proton beam. The slope of the line is a problem for the cryogenic supply of these magnets, which however can presumably be solved. The electron beam lines into and out of HERA require civil engineering work including two long slits of the HERA tunnel. A beam dump similar to the TESLA beam dump has to be foreseen, which would fit on the DESY site. Two types of superconducting quadrupoles for the new interaction region have to be provided with five magnets each and cryogenic supply. Beam pipes, support, power supplies, beam diagnostics and controls are required. In addition, faster kicker magnets are needed to provide the desired bunch spacing. In order to achieve the envisaged beam brightness, electron cooling in PETRA will most likely be required.

2.3.2 A detector for THERA

The electron–proton scattering kinematics governs the design of the THERA detector. Roughly speaking, there are three detector regions which have to match different requirements: the forward[5] part, where the final-state energies are limited by the proton beam energy, E_p; the central part, where particles with transverse momenta up to $\sqrt{s}/2$ can be produced; the backward part, where the final-state energies are limited by the electron beam energy, E_e. The forward part thus has to match similar criteria as at HERA, whereas the backward part has to cope with much higher energies. The central part bridges these two extremes.

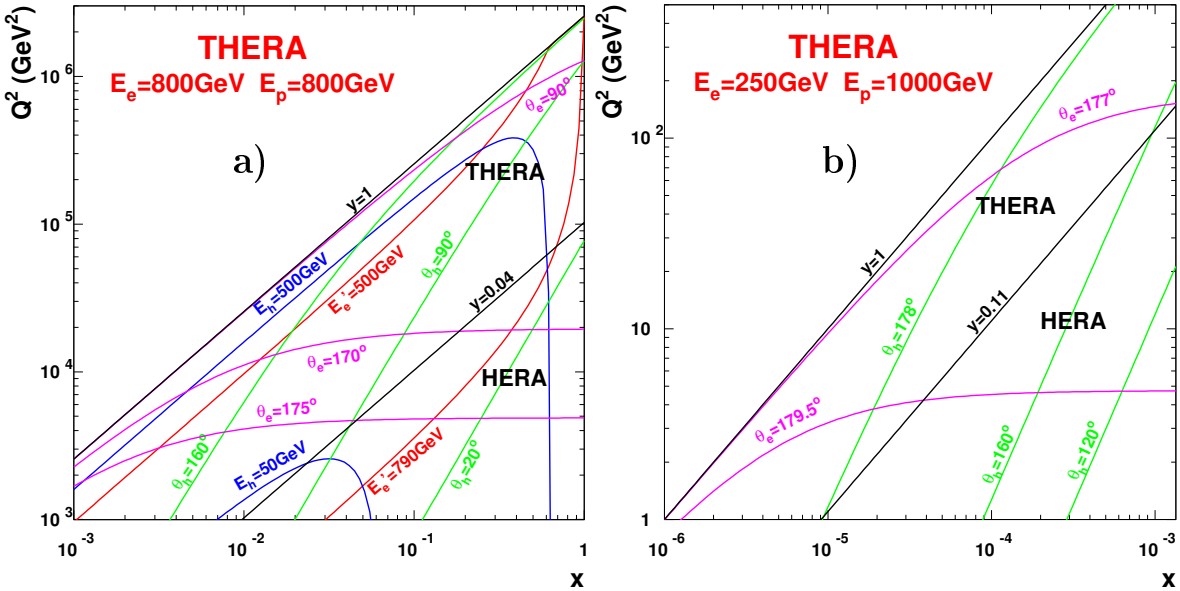

Figure 2.3.3: *Kinematic range covered by THERA, (a) at high x and Q^2 for $E_e = E_p = 800$ GeV ($\sqrt{s} = 1.6$ TeV), and (b) at low x and Q^2 for beam energies of $E_e = 250$ GeV and $E_p = 1$ TeV ($\sqrt{s} = 1$ TeV). The lines for $y = 0.04$ in (a) and $y = 0.11$ in (b) indicate the kinematic limit of HERA. Lines of constant E'_e (red), E_h (blue), θ_e (magenta) and θ_h (green) are indicated. In (b), E_h and E'_e are given approximately by yE_e and $(1-y)E_e$, respectively. Note that for low x both the electron and the jet are scattered into the backward region, illustrating the strong boost of the electron–quark system in this kinematic region.*

The coverage of the (x, Q^2) plane for DIS at large $Q^2 > 10^3\,\mathrm{GeV}^2$ is shown in Fig. 2.3.3a for the maximum THERA centre-of-mass energy envisaged (see Sect. 2.3.1.3). The final-state electrons have energies, E'_e, of hundreds of GeV and are scattered at backward and central angles, θ_e. The current jets emerge at a broad spectrum of angles, θ_h, hitting the forward, central and backward detector parts with energies, E_h,

[5] A coordinate system is defined according to the HERA conventions, with the origin in the interaction point (IP) and the z axis pointing in the proton beam direction, referred to as forward.

which are approaching E_p at highest x and E_e at highest y.

The kinematic properties of low-x reactions are illustrated in Fig. 2.3.3a. The most striking features of such events are the very small deflection of the electrons and their large energies of $E'_e \approx (1-y)\,E_e$, exceeding the corresponding values in the HERA backward region by one order of magnitude. As can be seen from this figure, Q^2 values of a few GeV^2 can be accessed only with electron scattering angles close to 180° (θ_e as large as 179.5° is e.g. required to reach $Q^2 = 4E_eE'_e\cos^2(\theta_e/2) \simeq 2\,\mathrm{GeV}^2$ at $y = 0.5$ for $E_e = 250\,\mathrm{GeV}$). Simultaneously, the current jets are also scattered into the backward direction, with energies $E_h \approx y\,E_e$.

The backward region of the THERA detector is therefore of central importance for low-x investigations and has to be newly designed, since the corresponding HERA detector components cannot provide the required energy containment and angular coverage. The extension in z of the very backward detector part (i.e. at largest θ) depends critically on the beam-pipe radius which can be as small as 2 cm because of the absence of synchrotron radiation from bends of the incoming electron beam near the interaction region. The beam-pipe will have exit windows with 2π azimuthal coverage to minimise shower development and multiple scattering.

Based on the experience of experimentation at HERA and a simulations of THERA DIS events and kinematics, a design study of the THERA detector has been performed [137].

The *operation* of the THERA experiment is envisaged in two phases aiming at low-x physics and high-Q^2 physics, respectively. Accordingly, the THERA detector is foreseen to be modular in its structure. Detectors near the beam-pipe and the extended backward part should be removable for high-luminosity operation, which will require the installation of focusing magnets as close as possible to the interaction point. Characteristic parameters of both phases are summarised in Table 2.3.2.

Magnetic field: A homogenous solenoidal magnetic field, extending over almost 10 m in z could be provided by the H1 and ZEUS coils which can be operated at 1–1.5 T. The mechanical stability of such an arrangement and the design of the support structure have not yet been investigated.

The *calorimeter* has to be almost 4π-hermetic in order to be able to reconstruct the longitudinal energy-momentum balance, $E-p_z$, which is essential for DIS event identification and reconstruction. The required energy resolutions are roughly $15\%/\sqrt{E(\mathrm{GeV})}$ for electromagnetic and $40\%/\sqrt{E(\mathrm{GeV})}$ for hadronic energy measurements, with additional constant terms of about 1%. These resolution requirements can be met by presently available calorimeter technology as e.g. employed by the HERA collaborations. In particular, one might consider to equip the forward and central calorimeter regions with the H1 LAr calorimeter, and to use the instrumented iron structure of the H1 detector. The reconstruction of forward-jet final states requires position reconstruction and energy flow measurements down to polar scattering angles of about 1°. Thus, a new calorimeter with enhanced granularity will have to be constructed for the very forward region, i.e. $\theta < 5°$ ('forward plug').

In the backward direction, the calorimeter must be able to provide energy and position measurement for the scattered electrons with energies close to the electron

	low-x configuration	high-Q^2 configuration	
electron beam energy, E_e	250 GeV	500 GeV	800 GeV
proton beam energy, E_p	1 TeV	500 GeV	800 GeV
c.m.s. energy, $\sqrt{s}$	1.0 TeV	1.0 TeV	1.6 TeV
luminosity [10^{30} cm^{-2} s^{-1}]	4	25	16
distance focusing magnet – IP	5 m	2 m	2 m
backward electron acceptance	$\theta_e < 179.7°$	$\theta_e < 175°$	$\theta_e < 175°$
forward calorimetric acceptance	$\theta_h > 1°$	$\theta_h > 5°$	$\theta_h > 5°$

Table 2.3.2: *Operation parameters of THERA. The first phase with standard beam energies and luminosity will focus on low-x physics. A subsequent, higher-luminosity phase is envisaged which will concentrate on high-Q^2 physics. In this high-Q^2 phase, both arms of TESLA are used for acceleration of electrons to achieve maximum energy. Note that the maximum Q^2 is given by $s = 4E_eE_p$. Choosing $E_e = E_p$ is favourable for maximising the luminosity (see Sect. 2.3.1). An electron energy of* 800 *GeV energy can be obtained after the TESLA power upgrade, while* 500 *GeV are available already in the first stage of TESLA.*

beam energy, at angles up to 179.7°. Furthermore, hadronic energy measurement and reliable electron/hadron separation are required in the same energy and angular range to fully cover low-x reactions, in which both the electron and the hadronic state are scattered into a narrow cone in the e beam direction (see Fig. 2.3.3a). These requirements necessitate a high-resolution, fine-grain calorimeter with sufficient depth to contain electron and hadronic energy deposits of several 100 GeV. Particularly stringent constraints are present for the calorimeter part close to the beam-pipe, which is envisaged to be constructed as a separate module ('backward plug').

Tracking: Tracks will be reconstructed in silicon strip detector telescopes near the beam-pipe and an arrangement of outer tracking detectors. These may consist of a cylindrical central chamber and, for example, of planes of straw-tube or drift-chamber detectors in the forward and the extended backward regions, with hit resolutions of about 150 μm.

Electron identification near $\theta_e = 179.5°$ will be achieved using a combination of the calorimetric information and the data from a track detector which has sufficient resolution to determine the charge of particles with momenta up to E_e and will be positioned in front of the backward plug calorimeter. Low-x charm and beauty physics requires the reconstruction of tracks with momenta of a few GeV at scattering angles up to 179°. It has been verified with simulation studies [138] that the required angular acceptance and momentum resolution can be provided using 6-inch silicon strip detectors with hit resolutions of about 20 μm. These detectors will be arranged in 5-plane modules, which are mounted around the beam pipe and cover the full range of polar and azimuthal angles. The backward tracker response was simulated in some detail, and resolutions of about 15 MeV for the $D^0 \to K\pi$ mass reconstruction and of about

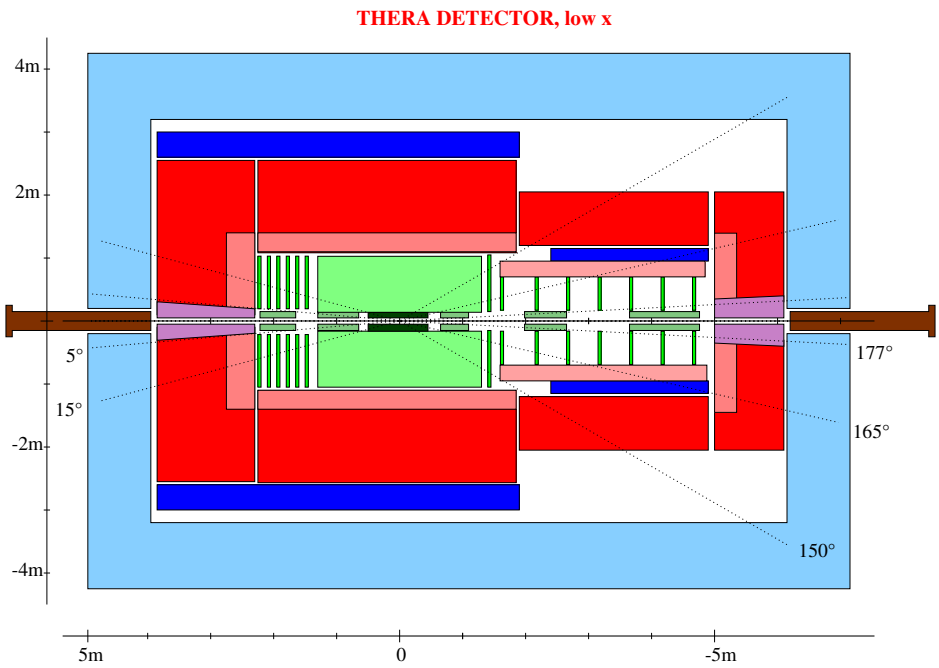

Figure 2.3.4: *Basic design of the THERA detector in the low-x configuration. The electrons enter from left, the protons from right. Around the beam-pipe, modules of 6-inch silicon strip detectors are positioned (dark-green). Tracking is complemented by planar and circular track chambers (light-green). Electromagnetic (pink) and hadronic (red) calorimetry ensures hermetic, accurate reconstruction of the final-state energy depositions. A homogenous, solenoidal field over 9 m length is provided by the large-diameter H1 coil and the smaller ZEUS coil (blue). The return yoke iron structure (light-blue) is instrumented for shower tail catching and muon detection. The focusing magnets (brown) are placed near the plug calorimeters (magenta).*

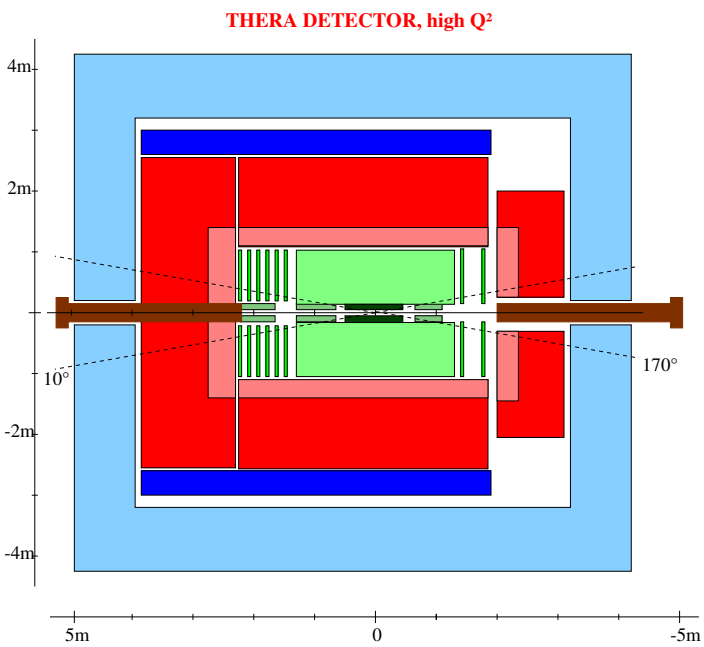

Figure 2.3.5: *Basic design of the THERA detector in the high-Q^2 configuration. This detector is similar in its basic layout to Figure 2.3.4, with the backward detector part and the ZEUS coil removed and the iron structure shortened correspondingly. Removal of the large/small angle trackers and the forward/backward plug calorimeters permits the focusing magnets to be placed much nearer to the interaction point than in the low-x phase.*

0.5 MeV for the $D^* - D^0$ mass difference were obtained. The tiny transverse size of the interaction spot (roughly 20 μm diameter) is of great advantage for momentum measurement and in particular for tagging heavy-flavour decays by reconstructing impact parameters and secondary vertices.

Muon chambers outside the calorimeter are required in the full acceptance range of the detector, preferentially also backwards at small angles for heavy-flavour physics.

Tagging of electrons and photons in the electron beam direction is necessary for luminosity measurements, control of radiative corrections and for identifying photoproduction events, in particular in the context of exclusive measurements. The detection of protons and neutrons in the proton beam direction is needed, or at least supportive, for investigations of diffractive reaction channels. It appears feasible to include these different tagging detectors in the interaction region; however, no effort has been made to design them at this stage.

It is concluded that low-x physics at THERA, while representing the challenge of measuring the scattered electron so close to the beam-pipe, can be studied with a detector design following the above considerations, as shown in Fig. 2.3.4. The design is sufficiently modular to allow for a detector reconfiguration suitable for the THERA high-Q^2 phase (see Fig. 2.3.5).

The construction of the THERA detector can be based on the large experience with the collider detectors at HERA and is not expected to exceed their cost.

2.4 Further Options

2.4.1 Electron–nucleus scattering

Deep inelastic scattering of nuclei is a classical way of studying the space-time picture of strong interactions, (see [139] for a recent review). So far DIS data on nuclei are only available for $x \gtrsim 0.003$, see e.g. Fig. 2.4.1 (reproduced from [139]).

The prime motive for using nuclear beams at THERA is to advance much deeper into the region of high parton densities than it would be possible in the electron–proton mode. Based on the dependence of various observables on the nucleon number, A, measurements at THERA would provide decisive tests and a number of valuable cross checks of various ideas about the QCD state in the high-density limit (for a summary see [141–143]). Effects to be investigated would include the saturation of gluon and quark densities [144, 145] (discussed in Sect. 2.2.1) or a large reduction of the nuclear gluon density [146], g_A, as compared to the incoherent sum $g_A = Ag_N$ of the individual nucleon densities, g_N (*leading-twist shadowing*). Indeed, the small-x gluon densities per unit area at central impact parameters in nuclei (i.e. at small transverse distances from the centre of the nucleus) are enhanced as compared to the nucleon case by a factor $(g_A/\pi R_A^2)/(g_N/\pi r_N^2) \approx A^{1/3} g_A/Ag_N$, which is as large as 6 for $A = 200$ if $g_A \approx Ag_N$ is assumed. The unitarity constraint (see eq. 2.2.1 for a nucleon target), requiring that the total inelastic cross section of the interaction of a small dipole with the nucleus cannot exceed πR_A^2 (*the black body limit*), implies the presence of large screening effects and nonlinear dynamics in eA scattering at THERA. In particular,

it implies that in the interaction of small colour-octet dipoles with nuclei at central impact parameters the gluon density per nucleon (i.e. the ratio of the gluon density averaged over a small range of central impact parameters and the number of nucleons, $A_{\rm eff}$, in the corresponding nuclear volume) cannot exceed [16, 147]

$$\left.\frac{x g_A(x,Q^2)}{A_{\rm eff}}\right|_{\rm central} \leq 3A^{-1/3}Q^2\,({\rm GeV}^2) \overset{A=200}{\approx} 0.5\,Q^2\,({\rm GeV}^2)\,. \qquad (2.4.1)$$

Note that this ratio would be equal to xg_N if the nucleon fields would add incoherently. The upper bound in eq. 2.4.1 can be compared e.g. with $xg_N(x{=}10^{-3}, Q^2{=}4\,{\rm GeV}^2) \geq 5$ in the current parton distribution fits. One concludes that strong modifications of the gluon field in heavy nuclei (as compared to the incoherent sum of the nucleon fields) appear to be unavoidable in a wide (x, Q^2) range to be covered by THERA.

A significant part of these modifications required to satisfy the unitarity constraints is the leading-twist reduction of the gluon and quark parton densities (shadowing) related to the leading-twist diffraction observed at HERA [146]. The rest should be due to nonlinear effects. The kinematic range where nonlinear effects are expected to be large is illustrated in Fig. 2.4.2 for scattering of small-size colour-triplet and colour-octet dipoles off nuclei, taking into account the leading-twist shadowing. For central impact parameters the limits are much stronger – the limit for the inclusive scattering off a nucleus with a given A corresponds to the limit at central impact parameters for a nucleus with $A' \approx A/3.5$, so that the inclusive curves for $A = 40$ are the same as the curves for central scattering off carbon (the subtraction of the contribution from scattering at peripheral impact parameters can be performed by studying cross sections for a series of nuclei, e.g. for $A, A/4, \ldots$ [141]). The interaction strength in this domain may reach values close to the black body limit and can be studied at THERA in a wide x range as a function of the parton density (i.e. the number of nucleons at the impact parameter

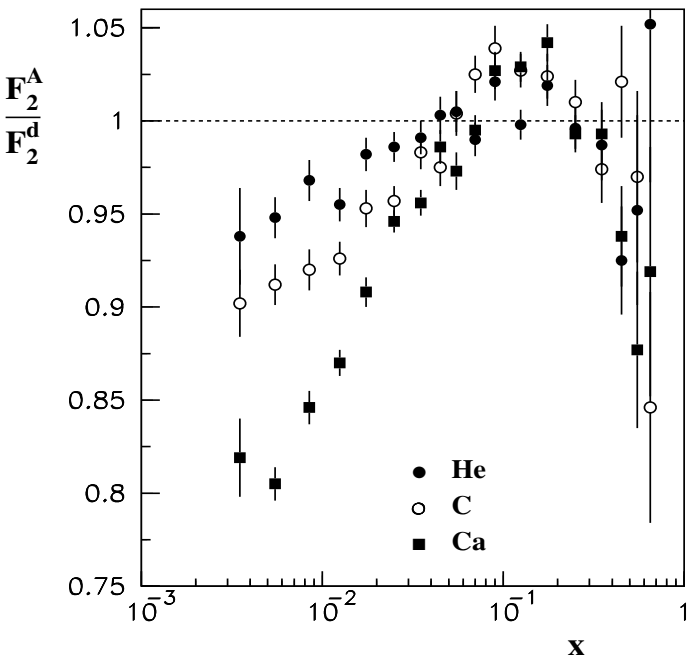

Figure 2.4.1: *NMC data [140] for the structure function ratio $F_2^{\rm A}/F_2^{\rm d}$ per nucleon for ^{4}He, ^{12}C and ^{40}Ca for $Q^2 \geq 0.7\,GeV^2$. THERA would extend these measurements by three orders of magnitude to $x \simeq 10^{-5}$.*

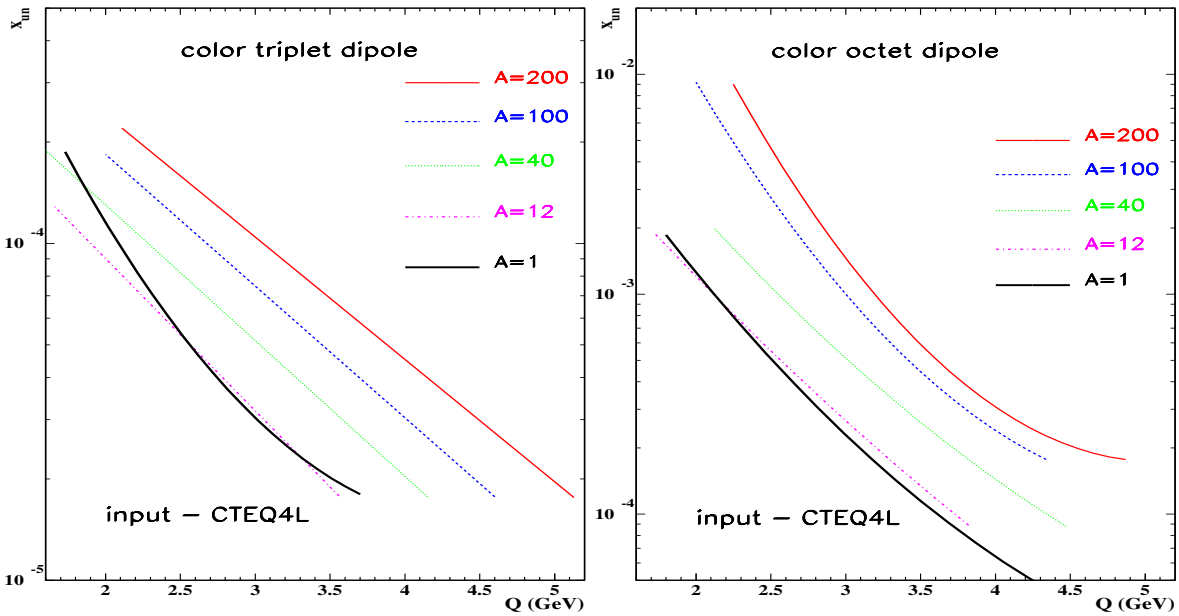

Figure 2.4.2: *Unitarity boundaries in the* $(x, \sqrt{Q^2})$*-plane for (a) the inelastic* $q\bar{q}$ *(colour triplet)–nucleus and (b) the* $q\bar{q}g$ *(colour octet)–nucleus cross sections for nuclei with* $A =$ 12, 40, 100 *and* 200. *The unitarity boundaries for the inelastic* $q\bar{q}$*– and* $q\bar{q}g$*–nucleon cross sections are indicated as black solid lines.*

of the probe), which is impossible for the case of ep scattering. In a number of models [148, 149] the shadowing in the leading twist is assumed to be small, resulting in a much larger range of (x, Q^2) where nonlinear effects should dominate (see plots in [142]).

One can see from the figure that the measurement of central scattering for $A = 40$ (which requires data from a set of isoscalar nuclei with $A \leq 40$ for the subtraction of the peripheral part) would access limits corresponding to inclusive scattering off nuclei with $A \sim 200$ and hence extend the Q^2 unitarity boundary by a at least a factor of two at x values of $\sim 10^{-4}$. This gain would allow the observation of nonlinear effects in a Q^2 range which is indisputably perturbative, at least for ep scattering.

It will be possible to reveal unambiguously the new high-density regime of DIS at small-x eA collisions via studies of a number of inclusive observables and the A-dependence of the properties of the final states. Several gold-plated observables are listed in the following. For illustration, expectations based on the black body limit scenario [16, 147, 150, 151] are considered (which is rather closely related to the saturation scenario [144, 145, 148, 149, 152, 153]), though nonlinear effects could tame the increase of the interaction strength before this limit is reached.

Inclusive observables

In the black body limit, the relation $F_2^A \propto 2\pi R_A^2 Q^2 \ln(1/x)$ holds for $Q^2 \leq Q^2_{\rm bbl}(x)$, where $Q^2_{\rm bbl}(x)$ denotes the maximal value of Q^2 for which the total inelastic cross section of the interaction of a small colour dipole of transverse size $\propto 1/Q$ with a heavy nucleus is equal to the black body limit, πR_A^2. The scale $Q^2_{\rm bbl}(x)$ increases with

A. The measurement of the scaling violation of $F_2^A(x, Q^2)$ provides direct access to the dynamics of the interaction of the small dipoles with nuclei and hence yields detailed information about the relevance of the black body limit for $\gamma^* A$ scattering. Direct tests of the onset of the black body regime in the gluon channel may be possible via measurements of $\sigma_L(eA)$ and the study of dijet production in $\gamma^* A$ scattering.

Another signal for approaching the black body limit would be an A dependence of the transverse momentum (p_t) spectrum of the partons: the average p_t rises with $Q^2_{\rm bbl}(x)$, $\langle p_t \rangle \sim Q_{\rm bbl}$ [148, 149], resulting in an A dependence of the leading hadron spectrum in the current fragmentation region at values of Feynman x close to one: the multiplicity will decrease with A [151] and the average p_t^2 at $x_F \sim 1$ should be proportional to $Q^2_{\rm bbl}$. Such a gross violation of the QCD factorisation theorem for leading hadron production in DIS will provide one of the model independent signals for the onset of the black body regime.

Diffractive observables

For experimental investigations, three classes of diffractive electron–nucleus interactions have to be considered: *diffractive dissociation* with meson production in the nucleus fragmentation region, *nuclear break-up* producing nuclear fragments (mostly neutrons and protons) in the forward direction, and *coherent scattering*, where the nucleus stays intact. The separation of these three classes from non-diffractive reactions is very similar to the selection of diffractive events in the ep case. The contribution of diffractive dissociation to the overall diffractive cross section is significantly smaller than in the ep case. The experimental signatures for this reaction class are similar to ep scattering since the energy flow in the forward direction is expected to have almost the same topology. Calorimetric coverage down to $\theta \lesssim 1°$ in the forward region (see Sect. 2.3.2) will allow the detection of most dissociative reactions. Nuclear break-up is expected to constitute about 10% of the coherent diffraction for a wide range of model parameters. Forward detectors similar to the forward neutron calorimeters (FNC) of the HERA collider experiments will be needed to distinguish these two processes [142].

Inclusive DIS diffraction provides a direct test of how close the interaction is to the black body limit, where the probability of coherent diffraction is close to 50% of the total cross section [150, 154–156]. The same is true for partial cross sections such as for charm production or dijet production in γA scattering. Moreover, since the interaction is stronger in the gluon channel, the diffractive cross section should be close to 50% of the corresponding total cross section in a wider (x, Q^2) range [146]. The differential cross section of diffractive production of states with mass $M_X^2 \leq Q^2_{\rm bbl}$ is also predicted in a model-independent way, see [151]. Another signature of the black body limit is that for $M_X^2 \leq Q^2_{\rm bbl}$ the production of high-p_t jets is strongly enhanced: $\langle (p_t^{\rm jet})^2 \rangle = 3M_X^2/20$.

Exclusive DIS diffraction, the production of vector mesons in the process $\gamma^* + A \to V + A$, provides a clean experimental signature if the V decay products are in the detector acceptance. This will be the case for light vector mesons if either Q^2 or $|t|$ (the square of the momentum transfer at the nucleon vertex) are sufficiently high, and for J/ψ and Υ mesons over the full kinematic range. The separation of coherent and incoherent events will require the same experimental techniques as for inclusive studies

and can in addition make use of the very steep diffractive peak expected for coherent processes. Exclusive DIS diffraction yields a direct answer to the fundamental question: Are heavy nuclei transparent for high-energy small objects like J/ψ or Υ mesons? In the region of $x \sim 0.02$, evidence for colour transparency was obtained [157] by the observation that the coherent J/ψ production amplitude is proportional to $AF_A(t)$, where $F_A(t)$ is the nuclear form factor. This colour transparency regime corresponds to the propagation of a small dipole through a thick target with very small absorption. At small $x \lesssim 0.01$, a qualitatively new phenomenon – colour opacity – is expected: a strong absorption of the small dipoles propagating through the nuclei. In the black body limit the increase of the cross section with A will be reduced to $A^{2/3}$ as compared to $A^{4/3}$ in the colour transparency limit. QCD also predicts the absolute cross section for the vector meson production in the black body limit. The THERA kinematic range would allow for studying the interplay of colour transparency and colour opacity in a wide (x, Q^2) range and distinguishing between various models of shadowing for the interaction of small dipoles. In particular, the eikonal model [144] leads to a much smaller colour opacity effect than the leading-twist models of gluon shadowing based on the dominance of gluons in the diffractive structure functions [146].

Measurements with deuteron beams (which probably can be polarised without installation of Siberian snakes using a novel technique suggested by A. Skrinsky [158]) would allow the investigation of low-x physics in reaction channels which cannot be induced by Pomeron exchange ('non-vacuum channels') by combining inclusive measurements and techniques of neutron tagging [141]. Measurements of non-vacuum exchange would be given by the structure function differences $F_2^p - F_2^n$ or $g_1^p - g_1^n$. Electron–deuteron scattering would also allow an interesting test of the Gottfried sum rule, $\int_0^1 (F_2^p - F_2^n)\, dx/x = 1/3 + 2/3 \int_0^1 (\bar{u} - \bar{d})\, dx$, in a new kinematic range.

To summarise, the use of nuclear beams would increase in a major way the THERA potential for the study of nonlinear QCD phenomena. Several measurements, especially in the diffractive channels, will determine in an unambiguous way whether the black body regime is reached and explore in detail a new QCD state of matter produced at small x. Most of these measurements will require rather modest luminosities of 1–10 pb^{-1} per nucleus [141]. It would be possible to explore the nonlinear regime in a Q^2 range extended by at least a factor of 2 with respect to ep scattering by performing measurements on a series of nuclei with $A \leq 40$, e.g. $A = 2, 4, 16, 40$.

2.4.2 Real photon–proton scattering

At a linear collider, laser light can be Compton-backscattered off the high-energy electron beam, offering the unique opportunity [159–161] to run THERA as a real-photon nucleon collider. As has been studied in detail in [159, 162], the luminosity for a γp machine depends on the distance z between the conversion region and the interaction point and also on the laser and electron beam helicities. An increase of z reduces the luminosity but also reduces the energy spread of the photon beam. A careful optimisation of the operation parameters such as the photon and electron beam helicities and the collision angle between the photon and proton beams is required. The basic

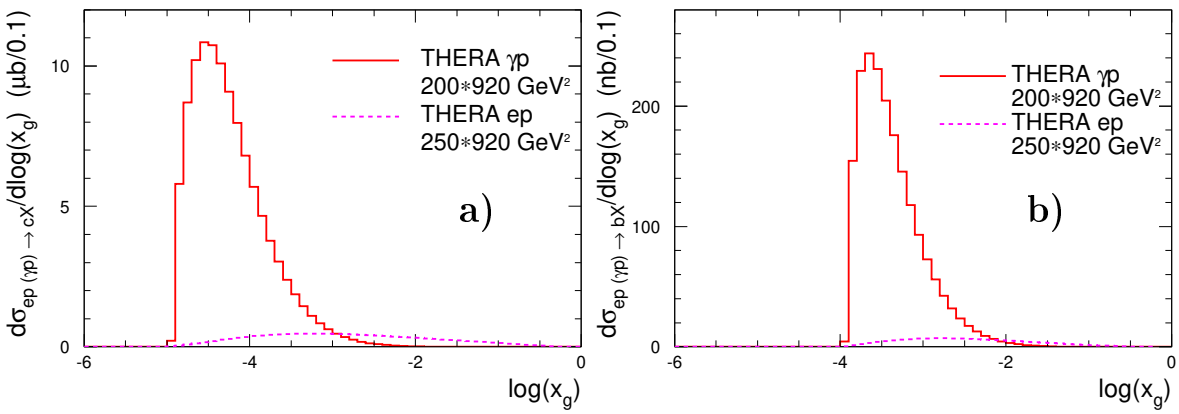

Figure 2.4.3: *Dependence of the differential cross section of (a) charm and (b) beauty production on x_g in γp and ep scattering at THERA.*

scheme for converting the TESLA electron beam into a high-energy photon beam is described in appendix I, *The Photon Collider at TESLA*, of this Technical Design Report. Given the much larger beam size of the protons, the interaction of the laser with the electron beam can happen several meters away from the photon–proton interaction point and thus outside of the detector. Photon–proton luminosities of order 30% of the electron–proton luminosities can be achieved.

Compton backscattering yields a beam of photons with about 80% of the electron beam energy on average, with a full width of approximately 15%. The resulting photon–proton interactions allow studies of many of the physics issues discussed above, e.g. heavy flavour production or photon structure, with much enhanced sensitivity. This is illustrated in Fig. 2.4.3 which compares the differential cross sections of charm and beauty production in γp scattering and in ep scattering as functions of the gluon fractional momentum in the proton, x_g. The cross section gain at low x_g is striking. A similar observation holds for the differential cross section with respect to the photon energy fraction, $x_\gamma^{\rm obs}$ (see eq. 2.2.2), carried by the produced dijet system in charm and beauty events as is shown in Fig. 2.4.4.

The main physics goals of a THERA-based γp collider [160, 163] are:

- a measurement of the total γp cross section at the TeV scale;
- high-statistics studies of heavy-quark production (roughly $10^8, 10^6, 10^2$ events per year for $c\bar{c}$, $b\bar{b}$, $t\bar{t}$ production);
- investigation of the partonic structure of real photons;
- single production of W bosons and top quarks;
- search for excited quarks (u^* and d^*) with masses up to 1 TeV;
- search for fourth-family quarks, Q, produced via anomalous γcQ, γuQ (Q=t_4, u_4), γsd_4 or γdd_4 couplings.

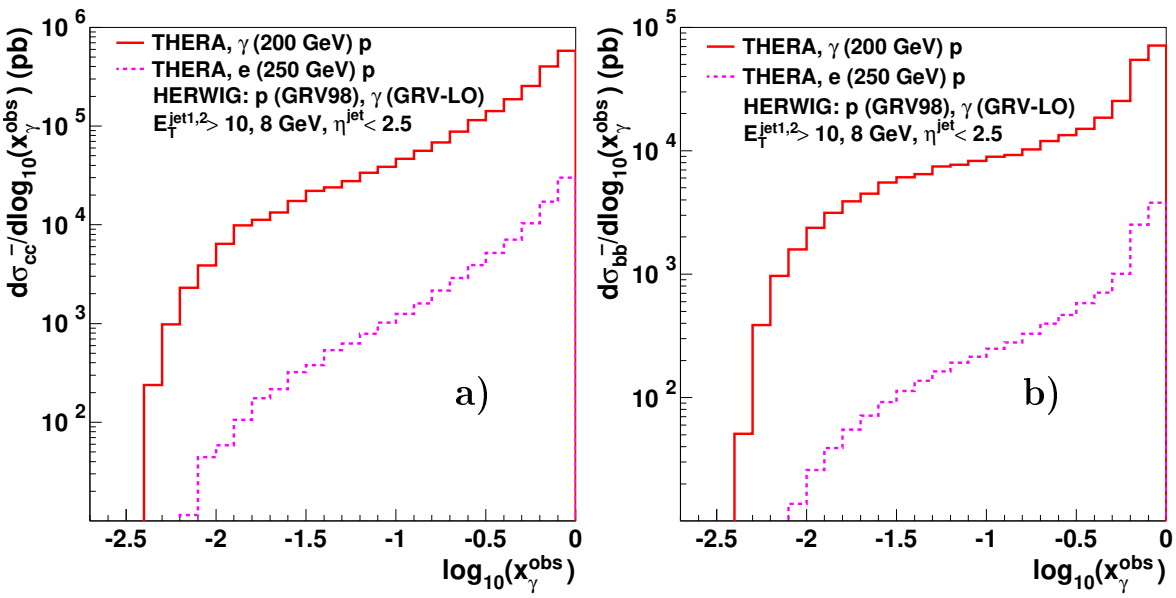

Figure 2.4.4: *Differential cross sections with respect to $x_\gamma^{\rm obs}$ for (a) charm and (b) beauty production for the γp and ep options of THERA.*

The photon polarisation will provide important additional information in all these measurements. In addition, a γp collider with a longitudinally polarised proton beam will be a powerful tool for investigating the spin structure of the proton.

Of particular interest is the photon–nucleus (γA) collider option of THERA (see Sect. 2.4.1 and [160, 163]) which, besides all the investigations mentioned above for the γp mode, allows for example detailed studies of quark–gluon plasma formation at very high temperature but relatively low nuclear density, or of multi-quark clusters in nuclei.

2.4.3 Polarised protons

The detailed study of the nucleon spin structure was initiated by the EMC muon experiment [164], which found that the quark contribution to the nucleon spin is surprisingly small and that hence the nucleon spin cannot be understood within the naive quark parton model. Since then a wealth of data from fixed-target experiments on spin structure has been accumulated and spin theory became much more sophisticated. The puzzling question of the nucleon spin composition is still unresolved (for the present status see [165]). The importance of extending the kinematic range of spin physics by an ep collider has been investigated and emphasised in a series of workshops on polarised ep physics at HERA [166–168].

In polarised DIS, the spin-dependent terms only make a small contribution to the total cross section. They can be extracted from measurements of cross section differences for interactions with opposite relative orientations of lepton and nucleon helicities, in which the spin-independent contributions cancel. A classic quantity is the

spin structure function g_1, which measures the weighted sum of polarised quark distribution functions Δq and is approximately related to the cross section asymmetry, $A_{||} = (\sigma_{\uparrow\downarrow} - \sigma_{\uparrow\uparrow})/(\sigma_{\uparrow\downarrow} + \sigma_{\uparrow\uparrow})$, by:

$$g_1 \simeq \frac{F_2}{2x} \cdot \frac{A_{||}}{\lambda_e \lambda_p} \cdot \frac{y^2 + 2(1-y)}{y(2-y)} \ . \tag{2.4.2}$$

Eq. 2.4.2 illustrates the need for high polarisations, λ_e and λ_p, and a preference for measurements at large values of y. The electron polarisation at TESLA will be high, $\lambda_e \simeq 0.8$. Polarisations $\lambda_p \simeq 0.6$ may be achieved in the HERA proton ring. From eq. 2.4.2 it can be deduced that integrated luminosities exceeding $100\,\mathrm{pb}^{-1}$ per polarisation state are necessary for studying the proton spin structure in a quantitative manner. Therefore, dedicated high-luminosity e–nucleus ring facilities are under discussion [169, 170] with typical energies of $\sqrt{s} \simeq 50\,\mathrm{GeV}$. High-statistics fixed target experiments are being carried out at CERN, DESY and SLAC and proposed to be pursued at TESLA [171].

The outstanding advantage of the THERA facility is the large extension of the kinematic range. Due to the very large centre-of-mass energy, $\sqrt{s} \simeq 1\,\mathrm{TeV}$, the Q^2 evolution can be tested, the x range expanded to much lower x and exploratory measurements be performed. In spin physics these comprise for example inclusive polarised deep inelastic scattering and spin asymmetries in jet and dijet production. For the first time, spin effects will be measurable in polarised DIS through electroweak asymmetries in CC and NC scattering.

The study of spin-dependent effects would be extended to low x and allow for a test of the Q^2 evolution of g_1 towards highest $Q^2 \simeq 10^4\,\mathrm{GeV}^2$. Important information on the spin structure can be obtained from data on the asymmetry in the production of two jets (dijets) or of two hadrons. The polarised gluon distribution ΔG can be accessed with dijet events, as was demonstrated in [172] for HERA operation with polarised protons. For THERA, the asymmetries, calculated with MEPJET and GSA, are about 6% at $x = 0.05$ and smaller than 0.5% for $x < 0.001$. A further source of information about gluon polarisation at low x is charm production which occurs with high cross section at THERA (see Sect. 2.2.2.4).

Inclusive measurements in DIS are sensitive to the sum of all quark flavours. To extract flavour-dependent spin information, one presently uses semi-inclusive scattering, an area being actively pursued in fixed-target experiments [165]. In the very high Q^2 range of THERA, however, CC interactions are a new and promising way to access flavour-specific spin information, independently of fragmentation effects which hinder semi-inclusive analyses. Thus CC scattering has been considered here as an example to illustrate the THERA potential for investigating the polarised proton structure at high Q^2.

In the CC e^+p and e^-p scattering cross sections, asymmetries can be defined as

$$A^{W^\mp} = \frac{d\sigma^{W^\mp}_{\uparrow\downarrow} - d\sigma^{W^\mp}_{\uparrow\uparrow}}{d\sigma^{W^\mp}_{\uparrow\downarrow} + d\sigma^{W^\mp}_{\uparrow\uparrow}} = \frac{\pm 2b g_1^{W^\mp} + a g_5^{W^\mp}}{a F_1^{W^\mp} \pm b F_3^{W^\mp}} \approx \frac{g_5^{W^\mp}}{F_1^{W^\mp}} \tag{2.4.3}$$

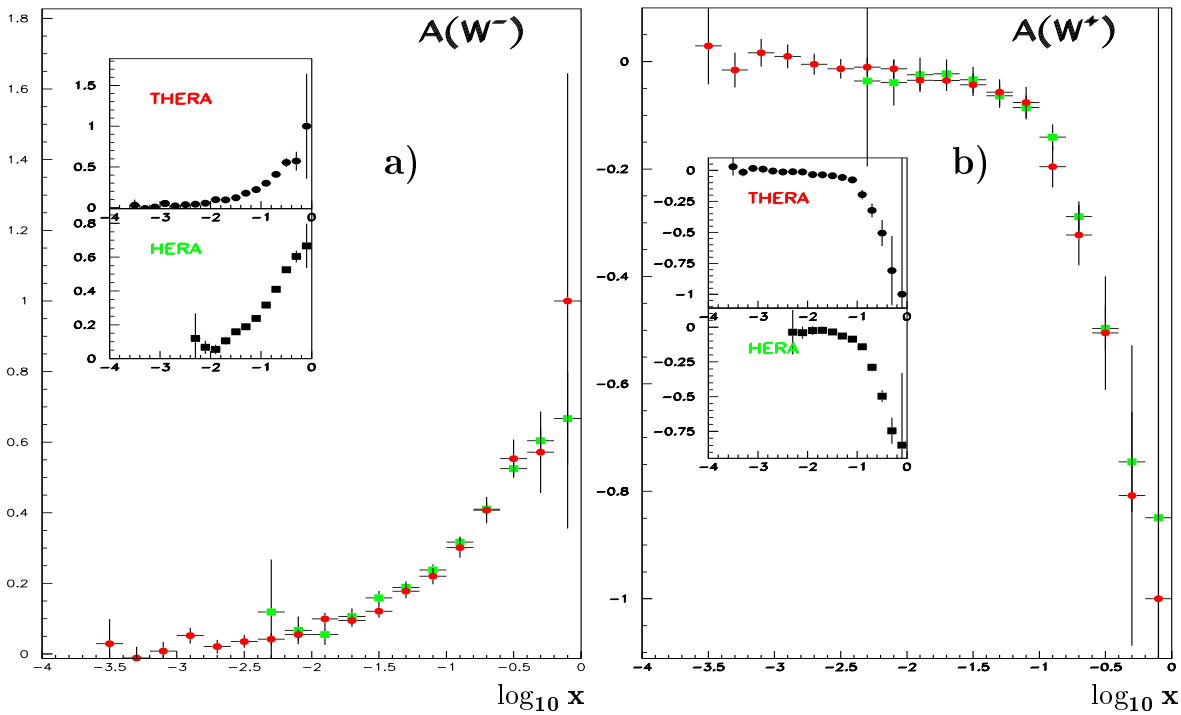

Figure 2.4.5: *Simulated measurements of (a) the asymmetry A^{W^-} and (b) of A^{W^+} in CC scattering as functions of x, as expected at the HERA and THERA facilities with polarised proton beams. Note that this representation hides the large differences in the Q^2 range of the HERA and THEA measurements, respectively.*

with $a = 2(y^2 - 2y + 2)$ and $b = y(2 - y)$, $g_5^{W^-} = \Delta u + \Delta c - \Delta\bar{d} - \Delta\bar{s}$ and $g_5^{W^+} = \Delta d + \Delta s - \Delta\bar{u} - \Delta\bar{c}$. A simulation study has been performed for the measurement of this asymmetry, requiring the total missing transverse momentum to exceed 12 GeV. From $A^{W^\mp}$ measurements, the new structure functions g_5 [173] can be extracted following the method used in [174]. The results for $A^{W^\pm}$ are shown in Fig. 2.4.5, for a luminosity of 100 pb^{-1} for each polarisation combination, assuming full polarisation. The error bars indicate the statistical precision of the measurement. The results are compared with simulated asymmetry measurements for polarised HERA operation, which will access lower Q^2 at a given x. THERA will allow such asymmetry measurements to be performed in the CC channel for x values down to below 10^{-3}, thus extending the range accessible to HERA by one order of magnitude in x and by even more compared to the projected electron–nucleus colliders. It is expected that $g_5^{W^+}$ can be measured at THERA in the region $x \gtrsim 10^{-2}$, while for electron scattering the asymmetries are large enough to allow for a measurement of $g_5^{W^-}$ down to $x \simeq 10^{-3}$. Both g_5 structure functions are related by a Bjorken sum rule which is valid for very large Q^2 [106].

If any deviation from the Standard Model is found, such as R-parity violating SUSY [175], leptoquarks [112] or instantons [176], it will be particularly interesting to study the helicity-specific properties of the corresponding objects in $\vec{e}\vec{p}$ scattering at THERA.

2.5 Summary

A new electron–proton collider, THERA, based on the linear accelerator TESLA and the proton ring HERA, can be built at DESY. With electron energies between 250 and 800 GeV and proton energies between 500 GeV and 1 TeV, THERA opens a new, unexplored energy range in deep inelastic lepton–nucleon scattering. Design considerations of the THERA facility lead to preliminary estimates of the achievable luminosity between 4 and $25 \times 10^{30}\,\mathrm{cm}^{-2}\,\mathrm{s}^{-1}$ (corresponding to annual luminosities between about $40\,\mathrm{pb}^{-1}$ and $250\,\mathrm{pb}^{-1}$), depending on the beam energies. Relying on the experience and some components of the H1 and ZEUS experiments at HERA, a detector design is presented which promises to allow successful experimentation at THERA at the required level of accuracy and in the full kinematic range. Operation of THERA can be envisaged to proceed in two phases, one dedicated to the physics at very low Bjorken x and the other to extremely high momentum transfers Q^2.

A study is presented of those physics subjects which, based on present results of HERA and theoretical extrapolations, are considered to most likely govern the future physics of deep inelastic scattering and photoproduction in the TeV energy range. Important aims of THERA are the understanding of strong interactions in the presence of high parton densities, a coherent description of the transition from small to large distances and the exploration of new particles and phenomena. The detection of the complete final state and high accuracy in the measurements allow a rich experimental and theoretical programme of research to be performed in the unexplored region. This will test QCD as the theory of strong interactions in much more depth than could be reached so far.

The results of the THERA studies [3] can be summarised as follows:

- The extension of the kinematic range down to $x \simeq 10^{-6}$ allows access to the high-parton-density domain and its detailed exploration in the deep-inelastic regime. Studies of the saturation phase of matter are expected to yield insight into the question of confinement. These studies require the measurements of inclusive DIS, of light and heavy vector meson production and of diffraction. These results will allow the transition from the perturbative to the non-perturbative QCD regime to be understood much better than presently.

- The measurement of proton structure functions at THERA will be essential for determining quark and gluon distributions in the proton in an unexplored kinematic region. This will be crucial for a consistent theoretical description of low-x phenomena, which so far is elusive, and also for understanding the interactions at hadron colliders and of highest-energy cosmic particles.

- The nature of diffraction will be studied in a much extended phase space region of the fractional proton longitudinal momentum loss, x_{IP}, and the ratio $\beta = x/x_{IP}$. The rise of the diffractive structure function $F_2^{D(3)}$ will be explored accurately, which, together with the inclusive F_2, constitutes one of the key measurements to investigate the properties of the saturation region.

- The study of forward-going jets at THERA is expected to reveal the mechanism for the evolution of QCD radiation at low x. The increased range for the Q^2 evolution of parton densities will allow a precision measurement of α_s to the level of 0.5%. This is accompanied by major theoretical efforts to calculate QCD to next-to-next-to-leading order.

- The total cross sections for charm and beauty production are expected to increase by factors of three and five, respectively, as compared to HERA. This will allow the structure functions F_2^c and F_2^b to be measured precisely, heavy-quark QCD predictions to be tested and the gluon distribution in the proton to be determined from the photon–gluon fusion process at much lower x.

- THERA will operate beyond the electroweak unification scale and is thus a truly 'electroweak interaction machine'. The measurement of neutral and charged current cross sections will allow the flavour content of the proton to be unfolded at very high Q^2 and large x, including the region near $x = 1$.

- THERA will probe physics beyond the Standard Model. In particular, leptoquarks or squarks in supersymmetry with R-parity violation can be produced and their couplings determined in a rather complete manner. THERA is very sensitive to four-fermion contact interactions and probes compactification scales up to about 2.8 TeV via t-channel exchange of Kaluza–Klein gravitons in models with large extra dimensions. THERA will extend the searches for excited fermions to masses of up to 1 TeV.

- The photon structure will be resolved at harder scales and lower x_γ. The higher cross section for heavy-flavour production will permit the charm and bottom content of the quasi-real and virtual photon to be explored. Photon structure studies at THERA will be complementary to the investigations in $\gamma\gamma$ and $e\gamma$ reactions at TESLA.

- The acceleration of nuclei in HERA allows the investigation of electron–nucleus scattering in a very high energy range. This may lead deep into the region of high parton densities at low x and to phenomena such as saturation or large leading-twist shadowing. In eA collisions, coherent diffraction is expected to represent about half of the total interaction cross section.

- A further option of THERA consists in colliding a high-energy quasi-monochromatic beam of real photons, produced by backscattering laser light off the TESLA electron beam, with the proton beam from HERA. This would extend the field of real-photoproduction studies into the TeV range and would allow for high-statistics studies of heavy-quark production at low x.

- Polarised proton–electron scattering at THERA allows the study of the spin structure of the proton and its theoretical interpretation in QCD to be extended into an hitherto unexplored kinematic range of low x and large Q^2.

THERA represents a unique, cost-effective facility for investigating the structure of matter down to distances of about 10^{-19} m. As such it continues the long tradition of lepton–nucleon scattering experiments. Similarly to HERA, which has been the ep companion of the pp and e^+e^- colliders Tevatron and LEP, the THERA facility will yield information complementary to the LHC and to TESLA, utilising the rich physics potential of deep inelastic scattering in the TeV range of energy.

References

[1] R.P. Feynman, *Photon–Hadron Interactions.* Benjamin, New York, 1972.

[2] G.A. Voss and B.H. Wiik, Ann. Rev. Nucl. Part. Sci. **44**, 413 (1994).

[3] *The THERA Book*, Report DESY-LC-REV-2001-062, 2001. `http://www.desy.de/~lcnotes`.

[4] H1 Coll., C. Adloff et al., *Deep inelastic inclusive ep scattering at low x and a determination of α_s.* Preprint DESY-00-181 (hep-ex/0012053), 2000. Subm. to Eur. Phys. J.

[5] ZEUS Coll., *Measurement of the proton structure function F_2 in e^+p collisions at HERA.* Subm. to *ICHEP2000*, Osaka, Japan, paper 412, 2000.

[6] V.N. Gribov and L.N. Lipatov, Sov. J. Nucl. Phys. **15**, 438 (1972);
G. Altarelli and G. Parisi, Nucl. Phys. **B 126**, 298 (1977);
Yu.L. Dokshitzer, Sov. Phys. JETP **46**, 641 (1977).

[7] ZEUS Coll., J. Breitweg et al., Phys. Lett. **B 487**, 53 (2000).

[8] ZEUS Coll., J. Breitweg et al., Eur. Phys. J. **C 6**, 603 (1999).

[9] H1 Coll., C. Adloff et al., Phys. Lett. **B 483**, 23 (2000).

[10] ZEUS Coll, J. Breitweg et al., Eur. Phys. J. **C 12**, 35 (2000).

[11] H1 Coll., *Measurement of $D^{*\pm}$ production and F_2^c in DIS.* Subm. to *ICHEP2000*, Osaka, Japan, paper 313, 2000.

[12] M.F. McDermott, *The dipole picture of small x physics: A summary of the Amirim meeting.* Preprint DESY-00-126 (hep-ph/0008260), 2000.

[13] A.H. Mueller, Nucl. Phys. **B 415**, 373 (1994).

[14] N.N. Nikolaev and B.G. Zakharov, Z. Phys. **C 49**, 607 (1991).

[15] N.N. Nikolaev and B.G. Zakharov, Z. Phys. **C 64**, 631 (1994).

[16] L. Frankfurt, W. Koepf and M. Strikman, Phys. Rev. **D 54**, 3194 (1996).

[17] E. Gotsman et al., *Has HERA reached a new QCD regime? (Summary of our view).* Preprint DESY-00-149 (hep-ph/0010198), 2000.

[18] M. Glück, S. Kretzer and E. Reya, Astropart. Phys. **11**, 327 (1999).

[19] J. Kwiecinski, A.D. Martin and A.M. Stasto, *Penetration of the earth by ultrahigh-energy neutrinos and the parton distributions inside the nucleon.* Preprint hep-ph/9905307, 1999. Talk at *34th Rencontres de Moriond: QCD and Hadronic Interactions*, Les Arcs, France.

[20] J. Bartels and H. Kowalski, *Diffraction at HERA and the confinement problem.* Preprint DESY-00-154 (hep-ph/0010345), 2000.

[21] L.V. Gribov, E.M. Levin and M.G. Ryskin, Phys. Rept. **100**, 1 (1983).

[22] A.H. Mueller and J. Qiu, Nucl. Phys. **B 268**, 427 (1986).

[23] E. Levin, *Low-x physics.* Preprint hep-ph/0010272, 2000. Talk at *Diffraction 2000, Centraro, Italy.*

[24] K. Golec-Biernat and M. Wüsthoff, Phys. Rev. **D 60**, 114023 (1999).

[25] A.M. Stasto, K. Golec-Biernat and J. Kwiecinski, Phys. Rev. Lett. **86**, 596 (2001).

[26] L. Frankfurt, M. McDermott and M. Strikman, *A fresh look at diffractive J/ψ photoproduction at HERA, with predictions for THERA.* Preprint hep-ph/0009086, 2000.

[27] B. Naroska, *New results on vector meson production at HERA.* Preprint hep-ex/0006010, 2000. Contrib. to *35th Rencontres de Moriond: QCD and High Energy Hadronic Interactions*, Les Arcs, France.

[28] J.A. Crittenden, *Exclusive Production of Neutral Vector Mesons at the Electron–Proton Collider HERA*, Springer Tracts in Modern Physics, Vol. 140. Springer, Berlin, Heidelberg, 1997.

[29] M.G. Ryskin, Z. Phys. **C 57**, 89 (1993).

[30] L.Frankfurt, W. Koepf and M. Strikman, Phys. Rev. **D 57**, 512 (1998).

[31] M.G. Ryskin et al., Z. Phys. **C 76**, 231 (1997).

[32] P. Merkel, *Diffractive Photoproduction of Heavy Vector Mesons at HERA.* Ph.D. Thesis, University of Hamburg, Report DESY-THESIS-1999-030, 1999.

[33] S.J. Brodsky et al., Phys. Rev. **D 50**, 3134 (1994).

[34] J.C. Collins, L. Frankfurt and M. Strikman, Phys. Rev. **D 56**, 2982 (1997).

[35] A.D. Martin, M.G. Ryskin and T. Teubner, Phys. Rev. **D 55**, 4329 (1997).

[36] J. Nemchik et al., Phys. Lett. **B 374**, 199 (1996).

[37] D.Yu. Ivanov, Phys. Rev. **D 53**, 3564 (1996).

[38] I.F. Ginzburg and D.Yu. Ivanov, Phys. Rev. **D 54**, 5523 (1996).

[39] S.J. Brodsky et al., Phys. Lett. **B 449**, 306 (1999).

[40] J.R. Forshaw and M.G. Ryskin, Z. Phys. **C 68**, 137 (1995).

[41] A.D. Martin, M.G. Ryskin and T. Teubner, Phys. Lett. **B 454**, 339 (1999).

[42] L.L. Frankfurt, M.F. McDermott and M. Strikman, JHEP **9902**, 002 (1999).

[43] A. Levy, Phys. Lett. **B 424**, 191 (1998).

[44] H1 Coll., C. Adloff et al., Z. Phys. **C 76**, 613 (1997).

[45] ZEUS Coll., J. Breitweg et al., Eur. Phys. J. **C 6**, 43 (1999).

[46] E.L. Feinberg and I.Y. Pomerantchuk, Nuovo Cim. Suppl. **III(4)**, 652 (1956);
F.E. Low, Phys. Rev. **D 12**, 163 (1975);
S. Nussinov, Phys. Rev. Lett. **34**, 1286 (1975).

[47] J. Bartels, J. Phys. **G 26**, 481 (2000).

[48] J. Kwiecinski, *Introduction to low x physics and diffraction.* Preprint hep-ph/0102018, 2001.

[49] P.V. Landshoff, *Pomeron physics: An update.* Preprint DAMTP-2000-122 (hep-ph/0010315), 2000. Talk at *Diffraction 2000*, Centraro, Italy.

[50] J.C. Collins, Phys. Rev. **D 57**, 3051 (1998). Erratum in Phys. Rev. **D 61** 019902 (2000).

[51] ZEUS Coll., J. Breitweg et al., Eur. Phys. J. **C 5**, 41 (1998);
H1 Coll., C. Adloff et al., *Diffractive jet production in deep-inelastic e^+p collisions at HERA.* Preprint DESY-00-174 (hep-ex/0012051), 2000. Subm. to Eur. Phys. J.

[52] W. Buchmüller, M.F. McDermott and A. Hebecker, Nucl. Phys. **B 487**, 283 (1997). Erratum in Nucl Phys. **B 500**, 621 (1997).

[53] W. Buchmüller, T. Gehrmann and A. Hebecker, Nucl. Phys. **B 537**, 477 (1999).

[54] J. Bartels, H. Lotter and M. Wüsthoff, Phys. Lett. **B 379**, 239 (1996). Erratum in Phys. Lett. **B 382**, 449 (1996);
J. Bartels, H. Jung and M. Wüsthoff, Eur. Phys. J. **C 11**, 111 (1999).

[55] E. Gotsman, E. Levin and U. Maor, Nucl. Phys. **B 493**, 354 (1997).

[56] G. Ingelman and P.E. Schlein, Phys. Lett. **B 152**, 256 (1985).

[57] E. Zijlstra and W. van Neerven, Nucl. Phys. **B 417**, 61 (1994). Erratum in Nucl. Phys **B 426**, 245 (1994);
J. Blümlein and S. Kurth, Phys. Rev. **D 60**, 014018 (1999);
E. Remiddi and J.A.M. Vermaseren, Int. J. Mod. Phys. **A 15**, 725 (2000);
J. Blümlein, Comput. Phys. Comm. **133**, 76 (2000);
S. Moch and J.A.M. Vermaseren, Nucl. Phys. **B 573**, 853 (2000).

[58] J. Santiago and F.J. Ynduráin, Nucl. Phys. **B 563**, 45 (1999).

[59] CTEQ Coll., H.L. Lai et al., Eur. Phys. J. **C 12**, 375 (2000).

[60] A.D. Martin et al., Eur. Phys. **C 4**, 463 (1998).

[61] M. Glück, E. Reya and A. Vogt, Eur. Phys. J. **C 5**, 461 (1998).

[62] J. Blümlein et al., *Twist-4 gluon recombination corrections for deep inelastic structure functions.* Preprint DESY-01-007 (hep-ph/0102025), 2000.

[63] J. Bartels and C. Bontus, Phys. Rev. **D 61**, 034009 (2000);
J. Bartels, C. Bontus and H. Spiesberger, *Factorization of twist four gluon operator contributions.* Preprint DESY-99-118 (hep-ph/9908411), 1999.

[64] M.A. Kimber, J. Kwiecinski and A.D. Martin, *Gluon shadowing in the low x region probed by the LHC.* Preprint PPP-01-01 (hep-ph/0101099), 2001.

[65] J. Bartels, K. Golec-Biernat and K. Peters, Eur. Phys. J. **C 17**, 121 (2000).

[66] E. Gotsman et al., *Higher twists and maxima for DIS on proton in high density QCD region.* Preprint TAUP-2644-2000 (hep-ph/0008280), 2000.

[67] E.A. Kuraev, L.N. Lipatov and V.S. Fadin, Sov. Phys. JETP **44**, 443 (1976).

[68] E.A. Kuraev, L.N. Lipatov and V.S. Fadin, Sov. Phys. JETP **45**, 199 (1977);
I.I. Balitsky and L.N. Lipatov, Sov. J. Nucl. Phys. **28**, 822 (1978).

[69] S. Catani and F. Hautmann, Nucl. Phys. **B 427**, 475 (1994).

[70] V.S. Fadin and L.N. Lipatov, Phys. Lett. **B 429**, 127 (1998).

[71] J. Blümlein, J. Phys. **G 19**, 1695 (1993);
J. Blümlein and W.L. van Neerven, Phys. Lett. **B 450**, 412 (1999);
J. Blümlein, *QCD evolution of structure functions at small x.* Preprint hep-ph/9909449, 1999. Lectures at *Ringberg Workshop: New Trends in HERA Physics*, Ringberg Castle, Tegernsee, Germany.

[72] G. Altarelli, R.D. Ball and S. Forte, Nucl. Phys. **B 575**, 313 (2000).

[73] R.K. Ellis, F. Hautmann and B.R. Webber, Phys. Lett. **B 348**, 582 (1995).

[74] M. Ciafaloni, Nucl. Phys. **B 296**, 49 (1988);
S. Catani, F. Fiorani and G. Marchesini, Phys. Lett. **B 234**, 339 (1990);
S. Catani, F. Fiorani and G. Marchesini, Nucl. Phys. **B 336**, 18 (1990);
G. Marchesini, Nucl. Phys. **B 445**, 49 (1995).

[75] H. Jung and L. Lönnblad, *Forward jet production at THERA*, in *The THERA Book* [3].

[76] S. Bethke, J. Phys. **G 26**, R27 (2000).

[77] C. Quigg, *Perspectives in high-energy physics.* Preprint hep-ph/0002080, 2000. Review Lecture at ICFA School on Instrumentation in Elementary Particle Physics, Istanbul, Turkey.

[78] S.I. Alekhin and A.L. Kataev, Nucl. Phys. **A 666**, 179 (2000).

[79] M. Klein, C. Pascaud and R. Wallny, *QCD analysis of structure function measurements*, in *The THERA Book* [3].

[80] W.L. van Neerven and A. Vogt, Nucl. Phys. **B 568**, 263 (2000).

[81] S. Larin, T. van Ritbergen and J.A.M. Vermaseren, Nucl. Phys. **B 427**, 41 (1994);
S. Larin et al., Nucl. Phys. **B 492**, 338 (1997);
A. Retey and J.A.M. Vermaseren, *Some higher moments of deep inelastic structure functions at next-to-next-to-leading order of perturbative QCD.* Preprint NIKHEF-2000-018 (hep-ph/0007294), 2000.

[82] W. van Neerven and A. Vogt, Nucl. Phys. **B 588**, 345 (2000);
W.L. van Neerven and A. Vogt, Phys. Lett. **B 490**, 111 (2000).

[83] B. Pötter, *High-p_t jet production*, in *The THERA Book* [3].

[84] H1 Coll., C. Adloff et al., *Measurement and QCD analysis of jet cross-sections in deep inelastic positron–proton collisions at $\sqrt{s}$ of* 300 *GeV.* Preprint DESY-00-145 (hep-ex/0010054), 2000. Subm. to Eur. Phys. J.

[85] ZEUS Coll., *Measurement of differential cross sections for dijet production in neutral current DIS at high Q^2 and determination of α_s.* Subm. to *ICHEP2000*, Osaka, Japan, paper 420, 2000.

[86] W.-K. Tung, *The heavy quark parton oxymoron – a mini-review of heavy quark production theory in pQCD*, in *Proc. 5th Int. Workshop on Deep Inelastic Scattering and QCD (DIS97), Chicago, IL, USA*, eds. J. Repond and D. Krakauer, p. 1014. American Institute of Physics, Woodbury, NY, 1997. Also in preprint hep-ph/9706480.

[87] A. Chuvakin, J. Smith and B.W. Harris, *Variable flavor number schemes versus fixed order perturbation theory for charm quark electroproduction.* Preprint YITP-SB-00-68 (hep-ex/0010350), 2000.

[88] H1 Coll., C. Adloff et al., Nucl. Phys. **B 545**, 21 (1999).

[89] ZEUS Coll., J. Breitweg et al., Eur. Phys. J. **C 6**, 67 (1999).

[90] H1 Coll., C. Adloff et al., Phys. Lett. **B 467**, 156 (1999);
ZEUS Coll., J. Breitweg et al., *Measurement of open beauty production in photoproduction at HERA.* Preprint DESY-00-166 (hep-ex/0011081), 2000. Subm. to Eur. Phys. J.

[91] S. Frixione et al., Nucl. Phys. **B 412**, 225 (1994);
M.L. Mangano, P. Nason and G. Ridolfi, Nucl. Phys. **B 373**, 295 (1992).

[92] P. Jankowski, M. Krawczyk and M. Wing, *Heavy quark production at THERA*, in *The THERA Book* [3].

[93] L Gladilin and I. Redondo, *Heavy quark production measurements at THERA*, in *The THERA Book* [3].

[94] S.P. Baranov and N.P. Zotov, *Heavy quark production in the semihard approach at THERA*, in *The THERA Book* [3].

[95] G. Marchesini et al., Comp. Phys. Comm. **67**, 465 (1992).

[96] B.W. Harris and J. Smith, Phys. Rev. **D 57**, 2806 (1998).

[97] J. Amundson et al., JHEP **0010**, 031 (2000). Also in hep-ph/0005221;
A. Chuvakin, J. Smith and B.W. Harris, *Variable flavor number schemes versus fixed order perturbation theory for charm quark electroproduction.* Preprint YITP-SB-00-68 (hep-ph/0010350), 2000.

[98] M. Buza and W.L. van Neerven, Nucl. Phys. **B 500**, 301 (1997);
R.S. Thorne and R.G. Roberts, *A variable number flavor scheme for charged current heavy flavor structure functions.* Preprint RAL-TR-2000-048 (hep-ph/0010344), 2000.

[99] V. Barone, C. Pascaud and F. Zomer, *A new global analysis of DIS data and the strange sea distribution*, in *Proc. Workshop on Light-Cone QCD and Nonperturbative Hadron Physics, Adelaide, Australia, 1999*, p. 167. 2000. Also in preprint hep-ph/0004268.

[100] E. Derman, Phys. Rev. **D 7**, 2755 (1973).

[101] M. Klein and T. Riemann, Z. Phys. **C 24**, 151 (1984).

[102] U.F. Katz, *Deep-Inelastic Positron–Proton Scattering in the High-Momentum-Transfer Regime of HERA*, Springer Tracts in Modern Physics, Vol. 168. Springer, Berlin Heidelberg, 2000.

[103] J. Blümlein et al., Z. Phys. **C 45**, 501 (1990).

[104] S. Kuhlmann et al., Phys. Lett. **B 476**, 291 (2000).

[105] J.G. Morfin, Nucl. Phys. Proc. Suppl. **79**, 664 (1999);
C. Albright et al., *Physics at a neutrino factory.* Report FERMILAB-FN-492 (hep-ex/0008064), 2000.

[106] W. van Neerven, *Precison tests of perturbative QCD at THERA.* Talk at THERA meeting, Hamburg, 2000.
`http://www.ifh.de/thera/agenda_18oct.html`.

[107] C.Y. Prescott et al., Phys. Lett. **B 77**, 347 (1978).

[108] A.F. Żarnecki, Eur. Phys. J. **C 17**, 695 (2000).

[109] W. Buchmüller, R. Rückl and D. Wyler, Phys. Lett. **B 191**, 442 (1987). Erratum in Phys. Lett. **B 448** 320 (1999).

[110] A.F. Żarnecki, *Leptoquark searches at future colliders.* Preprint hep-ph/0006335, 2000. Subm. to *ICHEP2000*, Osaka, Japan, abstract 193.

[111] A. Djouadi et al., Z. Phys. **C 46**, 679 (1990).

[112] P. Taxil, E. Tuğcu and J.M. Virey, Eur. Phys. J. **C 14**, 165 (2000).

[113] N. Arkani-Hamed, S. Dimopoulos and G. Dvali, Phys. Lett. **B 429**, 263 (1998);
N. Arkani-Hamed, S. Dimopoulos and G. Dvali, Phys. Rev. **D 59**, 086004 (1999).

[114] N. Arkani-Hamed and M. Schmaltz, Phys. Rev. **D 61**, 033005 (2000).

[115] K. Hagiwara, D. Zeppenfeld and S. Komamiya, Z. Phys. **C 29**, 115 (1985).

[116] M. Wing, *Inclusive dijet photoproduction and the resolved photon at THERA*, in *The THERA Book* [3].

[117] M. Krawczyk and A. Zembrzuski, *Prompt photon production at THERA*, in *The THERA Book* [3].

[118] U. Jezuita-Dabrowska and M. Krawczyk, *On the importance of the interference terms and longitudinal virtual photon contribution at THERA*, in *The THERA Book* [3].

[119] M. Stratmann, *Determining the spin structure of the photon at future colliders.* Preprint hep-ph/0006285, 2000. Contrib. to *DIS2000*, Liverpool.

[120] ZEUS Coll., J. Breitweg et al., Euro. Phys. J. **C 11**, 35 (1999);
ZEUS Coll., *The structure of the photon and the dynamics of resolved-photon processes in dijet photoproduction.* Subm. to *ICHEP2000*, Osaka, Japan, paper 418, 2000;
ZEUS Coll., *Measurement of dijet photoproduction at high transverse energies at HERA.* Subm. to *EPS-HEP99*, Tampere, Finland, paper 540, 1999.

[121] M. Krawczyk, A. Zembrzuski and M. Staszel, *Survey of present data on photon structure functions and resolved photon processes.* Preprint IFT-99-15 (hep-ph/0011083), 2000. Subm. to Phys. Rept.

[122] M. Klasen, *Jet photoproduction at THERA*, in *The THERA Book* [3].

[123] ZEUS Coll., M. Derrick et al., Phys. Lett. **B 348**, 665 (1995).

[124] S. Frixione, Z. Kunszt and A. Signer, Nucl. Phys. **B 467**, 399 (1996);
S. Frixione, Nucl. Phys. **B 507**, 295 (1997).

[125] S. Frixione and G. Ridolfi, Nucl. Phys. **B 507**, 315 (1997).

[126] L.E. Gordon and J.K. Storrow, Nucl. Phys. **B 489**, 405 (1997).

[127] M. Glück, E. Reya and A. Vogt, Phys. Rev. **D 45**, 3986 (1992).

[128] M. Glück, E. Reya and A. Vogt, Phys. Rev. **D 46**, 1973 (1992).

[129] P. Aurenche, J.P. Guillet and M. Fontannaz, Z. Phys. **C 64**, 621 (1994).

[130] G.A. Schuler and T. Sjöstrand, Z. Phys. **C 68**, 607 (1995).

[131] A. Piwinski, *Intrabeam scattering*, in *Proc. 9th Int. Conf. on High Energy Accelerators, Stanford (1974)*, p. 405. 1975.

[132] J. Maidment. Private communication, 2001.

[133] K. Balewski et al., Nucl. Instrum. Meth. **A 441**, 274 (2000).

[134] T. Sen, *Crossing angle option for HERA.* Report DESY-HERA-96-02, 1996.

[135] M. Tigner, B. Wiik and F. Willeke, *An electron–proton collider in the TeV range*, in *Proc. IEEE Particle Accelerator Conference, San Francisco*, p. 2910. 1991.

[136] R. Brinkmann and M. Dohlus, *A method to overcome the bunch length limitations on β_p^* for electron–proton colliders.* Report DESY-M-95-11, 1995.

[137] J. Crittenden et al., *A detector for THERA*, in *The THERA Book* [3].

[138] L. Gladilin et al., *The backward silicon tracker for THERA*, in *The THERA Book* [3].

[139] G. Piller and W. Weise, Phys. Rept. **330**, 1 (2000).

[140] New Muon Coll., P. Amaudruz et al., Nucl. Phys. **B 441**, 3 (1995).

[141] M. Arneodo et al., *Nuclear beams in HERA*, in *Proc. Workshop on Future Physics at HERA*, eds. G. Ingelman, A. De Roeck and R. Klanner, p. 887. Hamburg, Germany, DESY, 1996.

[142] L. Frankfurt and M. Strikman, *Small-x phenomena in eA collisions*, in *The THERA Book* [3].

[143] *Proc. Nuclear Theory Summer Meeting on eRHIC*, eds. L. McLerran and R. Venugopalan, 2000. Report BNL-52606.

[144] A.H. Mueller, Nucl. Phys. **B 335**, 115 (1990).

[145] E. Iancu, A. Leonidov and L. McLerran, *Nonlinear gluon evolution in the color glass condensate. I.* Preprint SACLAY-T00-166 (hep-ph/0011241), 2000.

[146] L. Frankfurt and M. Strikman, Eur. Phys. J. **A 5**, 293 (1999).

[147] L. Frankfurt, V. Guzey and M. Strikman, J. Phys. **G 27**, R23 (2001).

[148] L. McLerran and R. Venugopalan, Phys. Rev. **D 50**, 2225 (1994).

[149] L. McLerran and R. Venugopalan, Phys. Rev. **D 59**, 094002 (1999).

[150] V.N. Gribov, Sov. Phys. JETP **30**, 709 (1970).

[151] M. McDermott et al., Eur. Phys. J. **C 16**, 641 (2000).

[152] A.H. Mueller, Nucl. Phys. **B 558**, 285 (1999).

[153] Y.V. Kovchegov, A.H. Mueller and S. Wallon, Nucl. Phys. **B 507**, 367 (1997).

[154] N.N. Nikolaev, B.G. Zakharov and V.R. Zoller, Z. Phys. **A 351**, 435 (1995).

[155] L.L. Frankfurt and M.I. Strikman, Phys. Lett. **B 382**, 6 (1996).

[156] E. Gotsman et al., Phys. Lett. **B 492**, 47 (2000).

[157] B.H. Denby et al., Phys. Rev. Lett. **52**, 795 (1984).

[158] A. Skrinsky, *Prospects for polarized electron nuclei colliders*, in *Proc. Workshop on Physics With Electron Polarized Ion Collider (EPIC99)*, eds. L.C. Bland, J.T. Londergan and A.P. Szczepaniak. 1999.

[159] A.K. Çiftçi et al., Nucl. Instrum. Meth. **A 365**, 317 (1995).

[160] R. Brinkmann et al., *Linac-ring type colliders: Fourth way to TeV scale.* Preprint DESY-97-239 (physics/9712023), 1997.

[161] S. Sultansoy, *The post-HERA era: Brief review of future lepton hadron and photon hadron colliders.* Preprint DESY-99-159 (hep-ph/9911417), 1999.

[162] S.F. Sultanov, *Prospects of the future ep and γp colliders: Luminosity and physics.* Report IC/89/409, ICTP, Trieste, 1989.

[163] S. Sultansoy, Turkish J. Phys. **22**, 575 (1998).

[164] EMC Coll., J. Ashman et al., Phys. Lett. **B 206**, 364 (1988);
EMC Coll., J. Ashman et al., Nucl. Phys. **B 328**, 1 (1989).

[165] N.C.R. Makins, *Spin physics.* Talk at *DIS2000*, Liverpool, `hep.ph.liv.ac.uk/~disproc/plenary1/makins.ps.gz`, 2000;
U. Stösslein, *Summary of the spin programme (PWG1).* Talk at *DIS2000*, Liverpool, `hep.ph.liv.ac.uk/~disproc/plenary2/PWG1/stoesslein`, 2000.

[166] *Proc. Workshop on Future Physics at HERA*, eds. G. Ingelman, A. De Roeck and R. Klanner, 1996.

[167] *Proc. Workshop Deep Inelastic Scattering off Polarized Targets: Theory Meets Experiment*, ed. J. Blümlein et al., Report DESY-97-200, 1997.

[168] A. Deshpande, *The physics case for polarized protons at HERA*, in *Proc. Workshop on Polarized Protons at High Energies – Accelerator Challenges and Physics Opportunities*, eds. A. De Roeck, D. Barber and G. Rädel. 1999.

[169] *An electron ring collider at RHIC.* Proc. *2nd eRHIC Workshop*, Yale, 2000. Report BNL-52592.

[170] *An electron ring at RHIC and EIC.* Proc. *2nd Workshop on an Electron Ion Collider (EIC)*, Boston, 2000.

[171] TESLA-N Study Group, M. Anselmino et al., *Electron scattering with polarized targets at TESLA.* Preprint DESY-00-160 (hep-ph/0011299), 2000. Also in this volume.

[172] A. De Roeck et al., Eur. Phys. J. **C 6**, 121 (1999).

[173] J. Blümlein, RIKEN Rev. **28**, 126 (2000). Also in hep-ph/9912550.

[174] J.G. Contreras, A. De Roeck and M. Maul, *A study on Δu and Δd in charged current events using polarized beams at HERA*, in *Proc. Workshop on Physics with Polarized Protons at HERA, Hamburg*, p. 103. 1998. Also in preprint hep-ph/9711418.

[175] J. Ellis, S. Lola and K. Sridhar, Phys. Lett. **B 408**, 252 (1997).

[176] N. Kochelev, *Instantons, spin crisis and high Q^2 anomaly at HERA*, in *Proc. Workshop on Physics with Polarized Protons at HERA, Hamburg*, p. 225. 1997. `http://www.desy.de/~gehrt/heraspin/proclist.html`.